

# Supplemental Material: Chiral degeneracies and Fermi-surface Chern numbers in bcc Fe

Daniel Gosálbez-Martínez,<sup>1,2</sup> Ivo Souza,<sup>1,3</sup> and David Vanderbilt<sup>4</sup>

<sup>1</sup>*Centro de Física de Materiales, Universidad del País Vasco, 20018 San Sebastián, Spain*

<sup>2</sup>*Donostia International Physics Center, 20018 San Sebastián, Spain*

<sup>3</sup>*Ikerbasque Foundation, 48013 Bilbao, Spain*

<sup>4</sup>*Department of Physics and Astronomy, Rutgers University, Piscataway, New Jersey 08854-8019, USA*

**Note:** This PDF document contains a large number of pages and figures, and is best viewed electronically. By flipping pages in single-page (or fullscreen) mode a simple animation effect is obtained for each sequence of snapshots.

## I. CHIRAL TOUCHING BETWEEN FERMI SHEETS INDUCED BY MAGNETIZATION PRECESSION

Figure S1 shows the Fermi contours of bands nine and ten of bcc Fe on the  $\Gamma$ NH ( $k_z = 0$ ) plane in Fig. 3, calculated with the magnetization pointing along  $[001]$ . The blow-up on the right shows the gluing-together of sheets 9 and  $10_2$  at two separate points along a degeneracy loop protected by mirror symmetry, see Sec. VI.B.1. The gluings with sheet 9 render ill-defined the Chern numbers of the low-symmetry pockets ( $10_2, 10_3, 10_4, 10_5$ ), as discussed in Sec. VI.B.3.

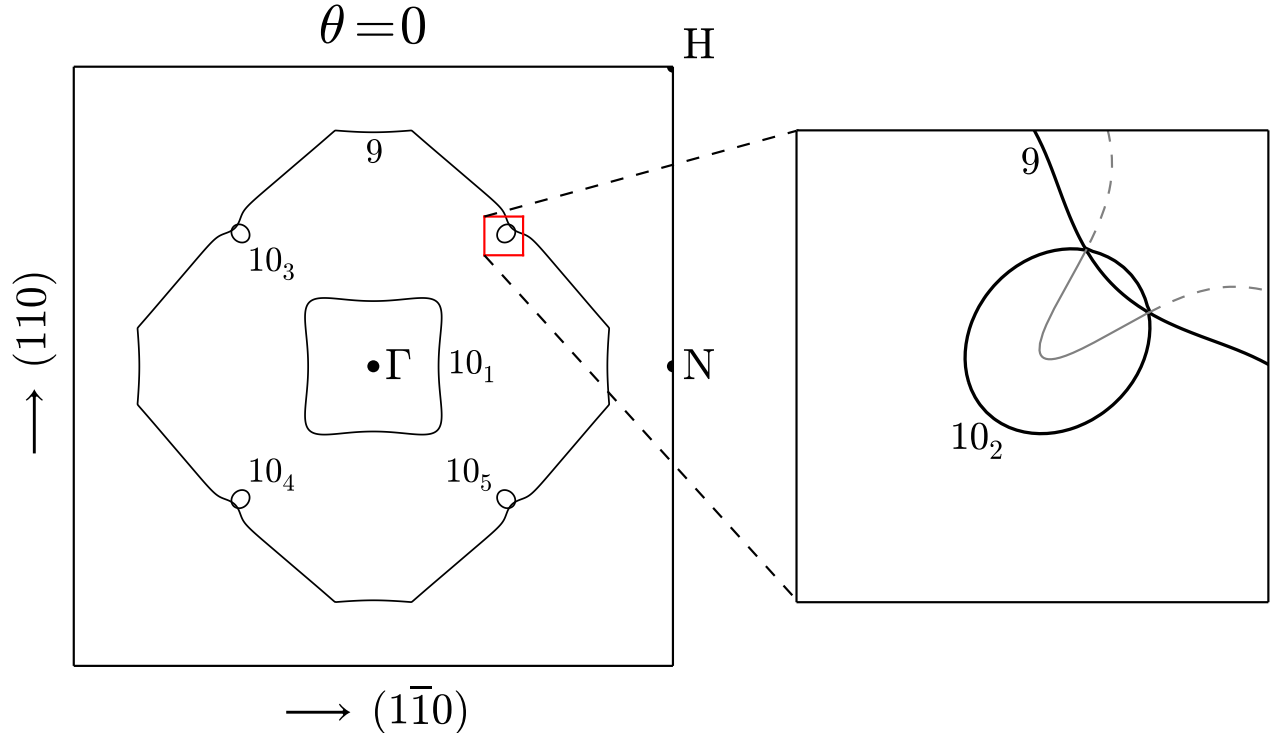


FIG. S1. Left: Fermi contours of bands nine and ten on the  $\Gamma$ NH Brillouin-zone slice at  $k_z = 0$ , with the magnetization pointing along  $[001]$  (polar angle  $\theta = 0$ ). Right: Detail showing the gluing points between sheets 9 and  $10_2$  along a nodal ring. The solid-line portion of the nodal ring is below the Fermi level, and the dashed-line portions are above.

In Fig. S2 the magnetization has been tilted by  $20^\circ$  towards the  $[100]$  axis, breaking the mirror symmetry. As a result the nodal rings have been reduced to a few Weyl points, and the previously glued-together Fermi sheets became isolated, with well-defined Chern numbers given by the enclosed chiral charges (Sec. VI.B.3). For example, pocket  $10_2$  has Chern number  $+1$ , because it encloses a single touching point of negative chirality with the band below.

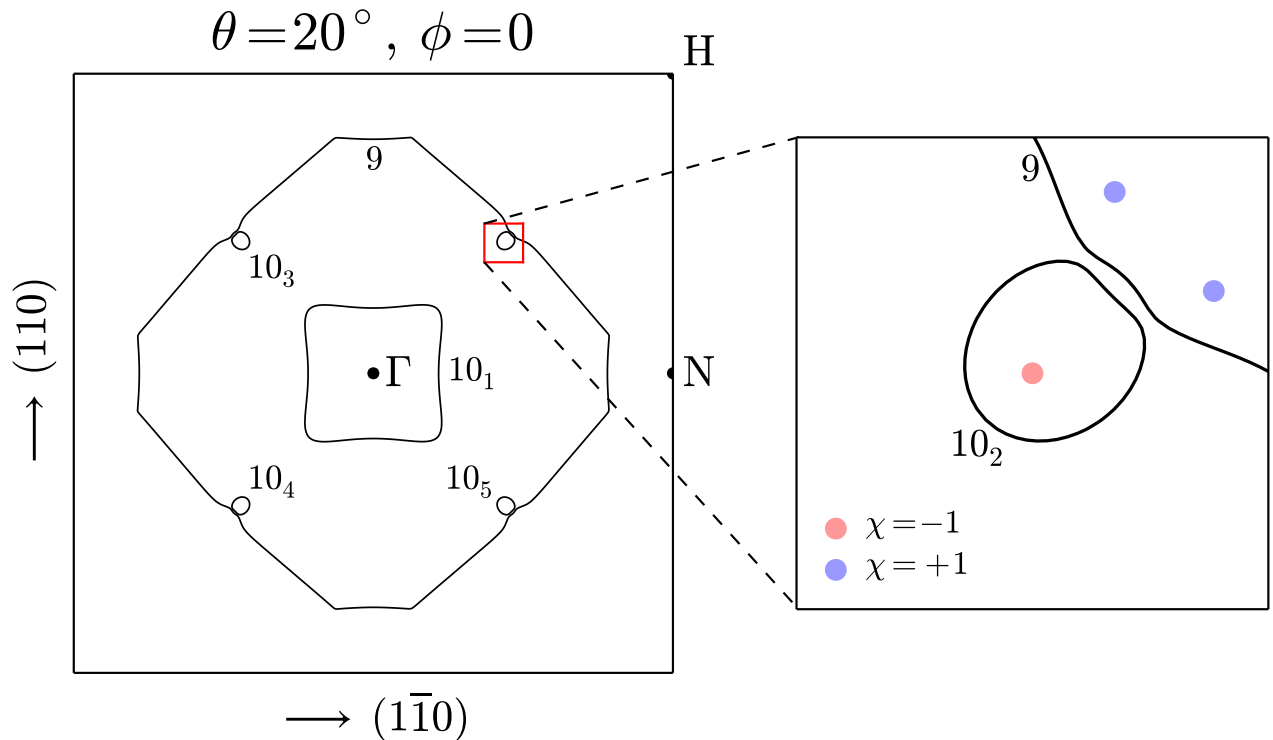


FIG. S2. Left: Fermi contours of bands nine and ten on the  $\Gamma$ NH Brillouin-zone slice at  $k_z = 0$ , with the magnetization tilted by  $20^\circ$  towards the  $[100]$  axis. Right: Detail showing the now-detached sheets 9 and  $10_2$ . The nodal ring has evaporated, leaving behind a few remnant Weyl points represented by the colored disks, with chiralities  $\chi$ .

The series of snapshots in Figs. S3-S19 depict the evolution of sheets 9 and  $10_2$ , and the motion of nearby remnant Weyl points (WPs), as the tilted magnetization precesses around  $[001]$  ( $\phi$  is the azimuthal precession angle). In order to see clearly the touching event between the two sheets at  $\phi \simeq 46^\circ$ , the Fermi contours are not drawn at exactly  $k_z = 0$ : in each snapshot the  $k_z$  coordinate of the contours is pinned to the WP that joins the two sheets at the critical angle (in practice  $k_z$  varies only slightly from one snapshot to the next, never deviating by more than  $0.004 \times 2\pi/a$  from  $k_z = 0$ ). The touching event at  $\phi \simeq 46^\circ$  leads to a transfer of Chern number between the two sheets, after which the Chern number of pocket  $10_2$  vanishes as it now encloses two WPs of opposite chirality. The two WPs merge together and annihilate at  $\phi \simeq 50^\circ$ .

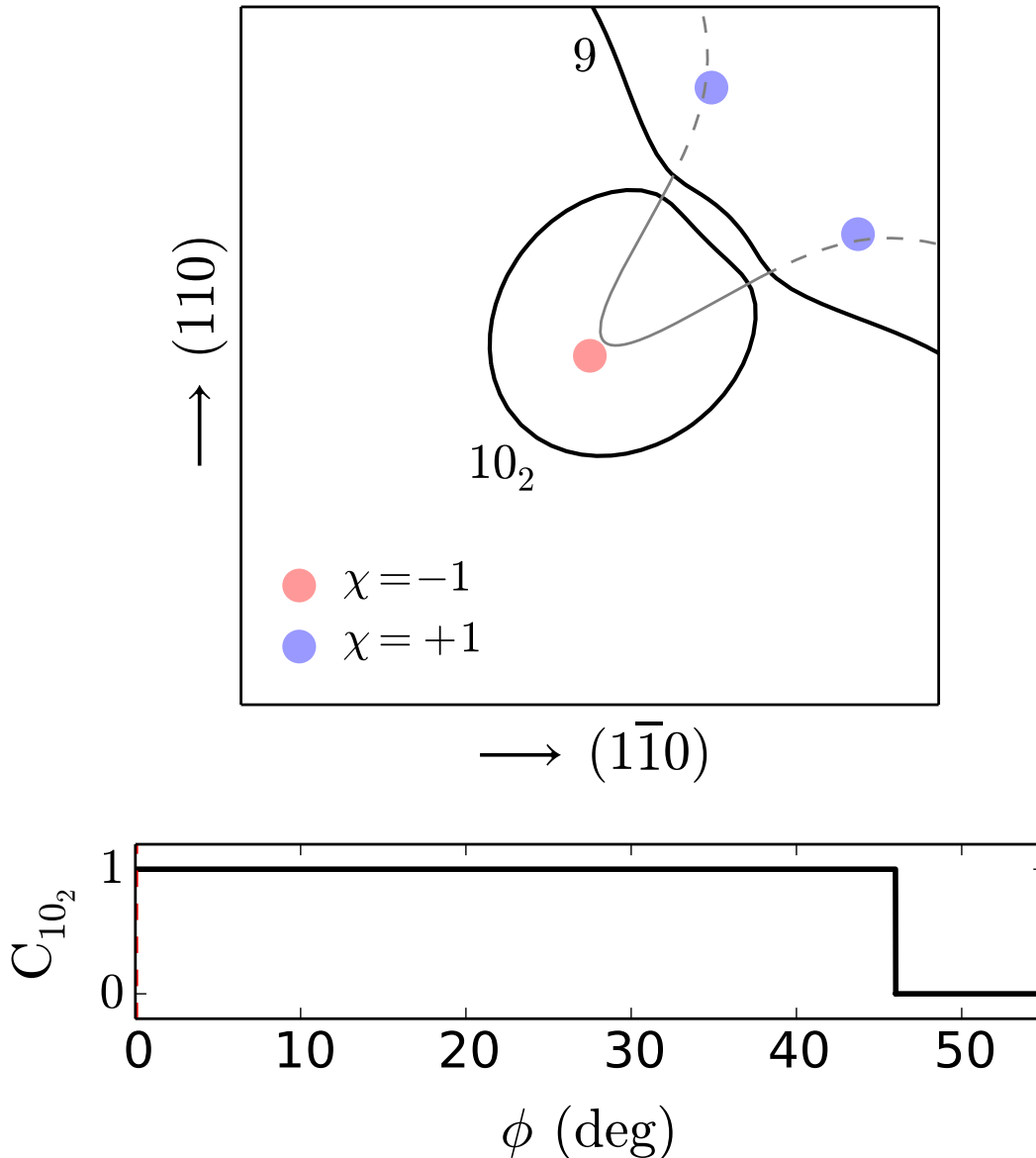


FIG. S3. Upper panel: Fermi contours of bands nine and ten, calculated with the magnetization tilted by  $20^\circ$  (the azimuthal angle  $\phi$  is indicated by the dashed red line in the lower panel). The remnant Weyl points are displayed as colored disks, and the evaporated nodal ring is shown as a guide to the eye. Lower panel: Chern number of pocket  $10_2$  versus  $\phi$ .

The series of snapshots in Figs. S3-S19 depict the evolution of sheets 9 and  $10_2$ , and the motion of nearby remanant Weyl points (WPs), as the tilted magnetization precesses around  $[001]$  ( $\phi$  is the azimuthal precession angle). In order to see clearly the touching event between the two sheets at  $\phi \simeq 46^\circ$ , the Fermi contours are not drawn at exactly  $k_z = 0$ : in each snapshot the  $k_z$  coordinate of the contours is pinned to the WP that joins the two sheets at the critical angle (in practice  $k_z$  varies only slightly from one snapshot to the next, never deviating by more than  $0.004 \times 2\pi/a$  from  $k_z = 0$ ). The touching event at  $\phi \simeq 46^\circ$  leads to a transfer of Chern number between the two sheets, after which the Chern number of pocket  $10_2$  vanishes as it now encloses two WPs of opposite chirality. The two WPs merge together and annihilate at  $\phi \simeq 50^\circ$ .

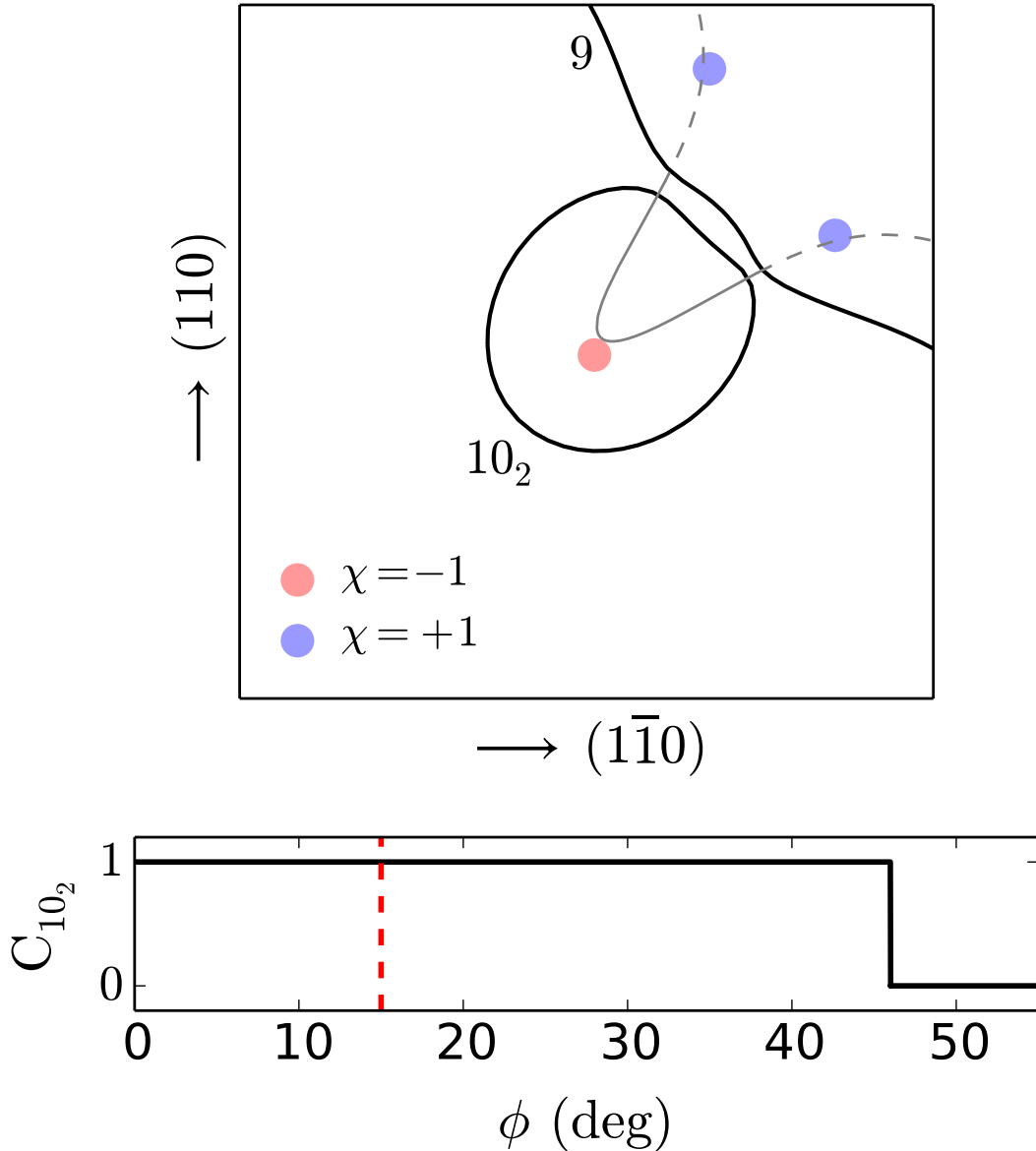


FIG. S4. Upper panel: Fermi contours of bands nine and ten, calculated with the magnetization tilted by  $20^\circ$  (the azimuthal angle  $\phi$  is indicated by the dashed red line in the lower panel). The remnant Weyl points are displayed as colored disks, and the evaporated nodal ring is shown as a guide to the eye. Lower panel: Chern number of pocket  $10_2$  versus  $\phi$ .

The series of snapshots in Figs. S3-S19 depict the evolution of sheets 9 and  $10_2$ , and the motion of nearby remanant Weyl points (WPs), as the tilted magnetization precesses around  $[001]$  ( $\phi$  is the azimuthal precession angle). In order to see clearly the touching event between the two sheets at  $\phi \simeq 46^\circ$ , the Fermi contours are not drawn at exactly  $k_z = 0$ : in each snapshot the  $k_z$  coordinate of the contours is pinned to the WP that joins the two sheets at the critical angle (in practice  $k_z$  varies only slightly from one snapshot to the next, never deviating by more than  $0.004 \times 2\pi/a$  from  $k_z = 0$ ). The touching event at  $\phi \simeq 46^\circ$  leads to a transfer of Chern number between the two sheets, after which the Chern number of pocket  $10_2$  vanishes as it now encloses two WPs of opposite chirality. The two WPs merge together and annihilate at  $\phi \simeq 50^\circ$ .

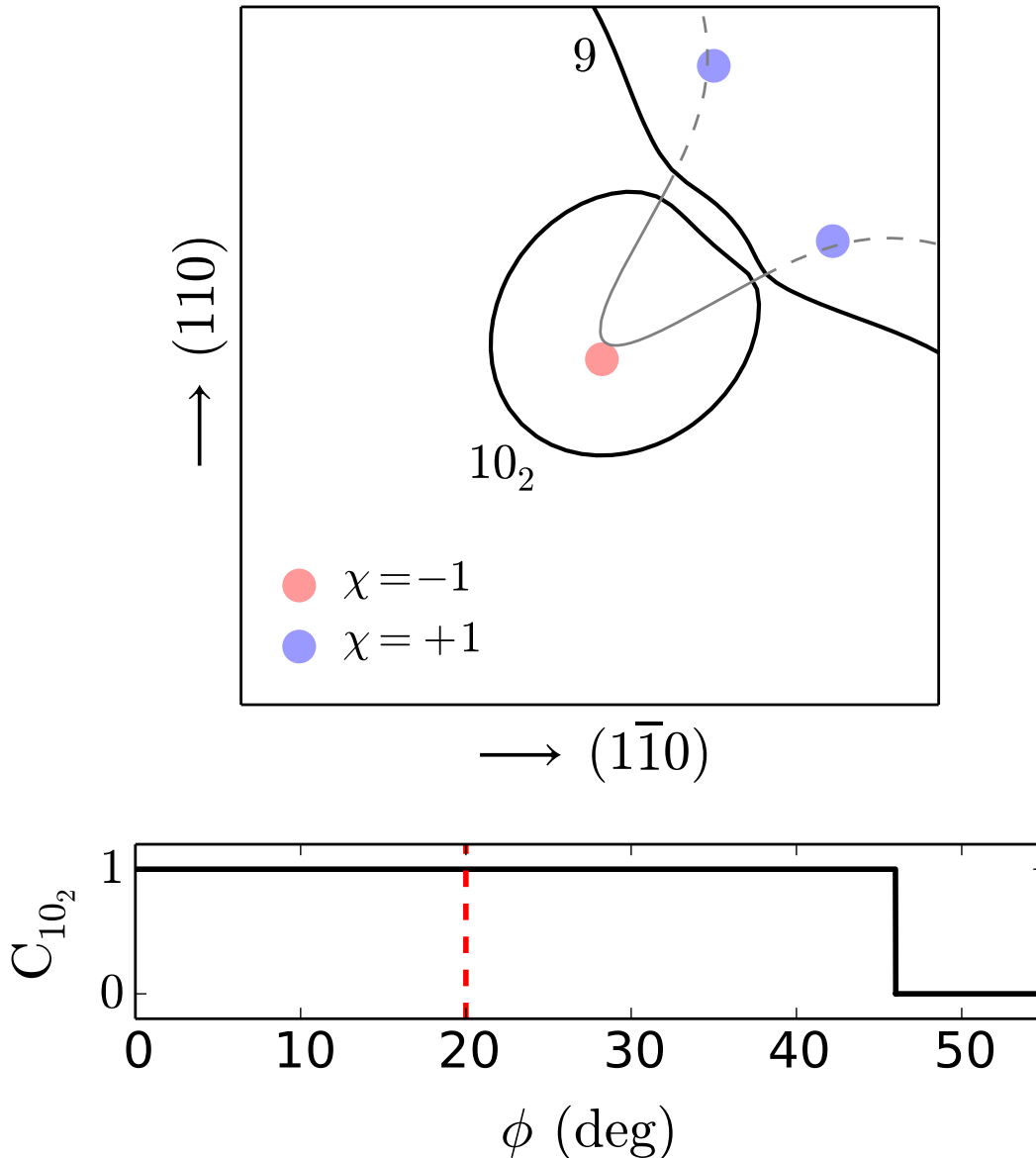


FIG. S5. Upper panel: Fermi contours of bands nine and ten, calculated with the magnetization tilted by  $20^\circ$  (the azimuthal angle  $\phi$  is indicated by the dashed red line in the lower panel). The remnant Weyl points are displayed as colored disks, and the evaporated nodal ring is shown as a guide to the eye. Lower panel: Chern number of pocket  $10_2$  versus  $\phi$ .

The series of snapshots in Figs. S3-S19 depict the evolution of sheets 9 and  $10_2$ , and the motion of nearby remanant Weyl points (WPs), as the tilted magnetization precesses around  $[001]$  ( $\phi$  is the azimuthal precession angle). In order to see clearly the touching event between the two sheets at  $\phi \simeq 46^\circ$ , the Fermi contours are not drawn at exactly  $k_z = 0$ : in each snapshot the  $k_z$  coordinate of the contours is pinned to the WP that joins the two sheets at the critical angle (in practice  $k_z$  varies only slightly from one snapshot to the next, never deviating by more than  $0.004 \times 2\pi/a$  from  $k_z = 0$ ). The touching event at  $\phi \simeq 46^\circ$  leads to a transfer of Chern number between the two sheets, after which the Chern number of pocket  $10_2$  vanishes as it now encloses two WPs of opposite chirality. The two WPs merge together and annihilate at  $\phi \simeq 50^\circ$ .

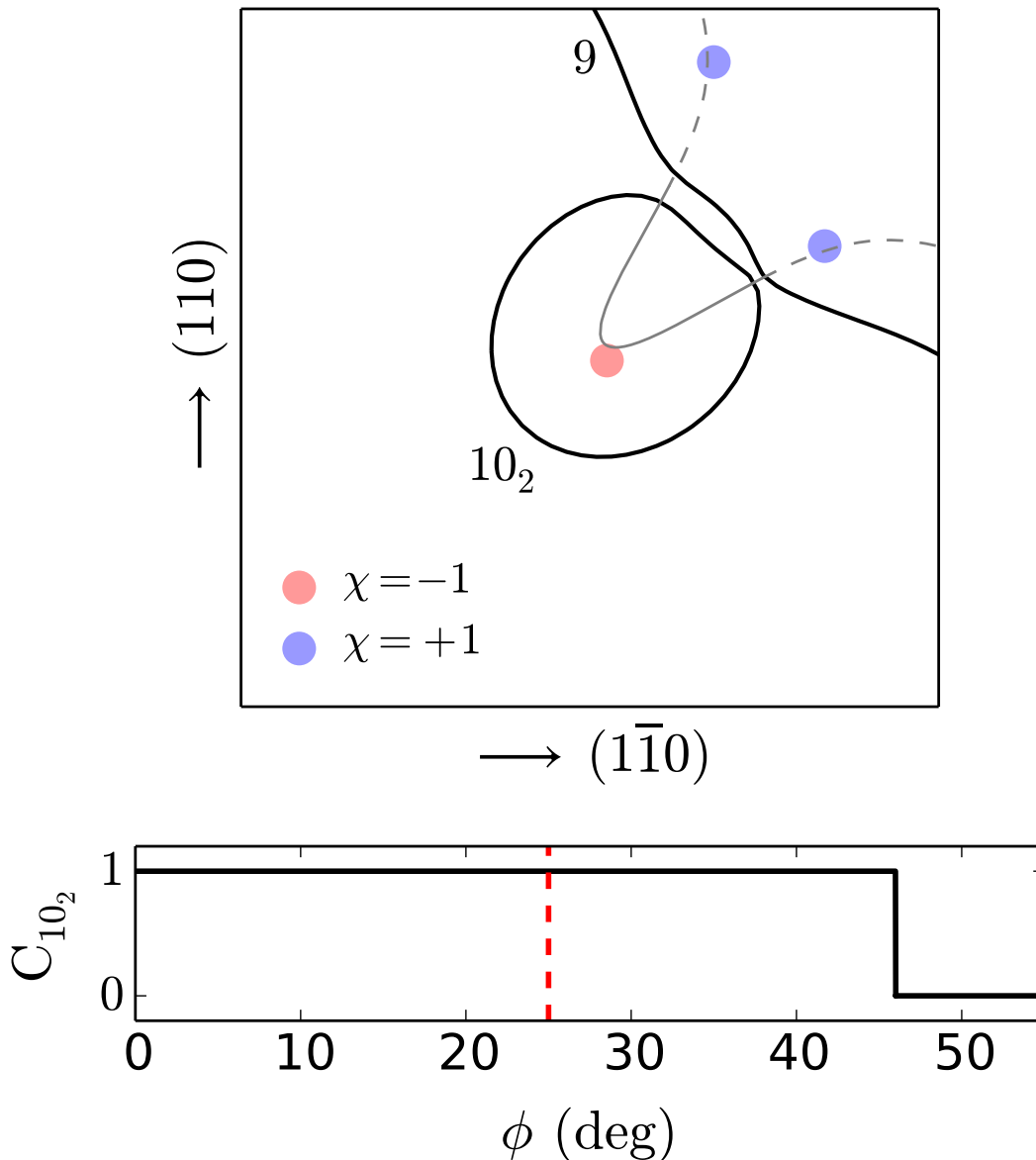


FIG. S6. Upper panel: Fermi contours of bands nine and ten, calculated with the magnetization tilted by  $20^\circ$  (the azimuthal angle  $\phi$  is indicated by the dashed red line in the lower panel). The remnant Weyl points are displayed as colored disks, and the evaporated nodal ring is shown as a guide to the eye. Lower panel: Chern number of pocket  $10_2$  versus  $\phi$ .

The series of snapshots in Figs. S3-S19 depict the evolution of sheets 9 and  $10_2$ , and the motion of nearby remanant Weyl points (WPs), as the tilted magnetization precesses around [001] ( $\phi$  is the azimuthal precession angle). In order to see clearly the touching event between the two sheets at  $\phi \simeq 46^\circ$ , the Fermi contours are not drawn at exactly  $k_z = 0$ : in each snapshot the  $k_z$  coordinate of the contours is pinned to the WP that joins the two sheets at the critical angle (in practice  $k_z$  varies only slightly from one snapshot to the next, never deviating by more than  $0.004 \times 2\pi/a$  from  $k_z = 0$ ). The touching event at  $\phi \simeq 46^\circ$  leads to a transfer of Chern number between the two sheets, after which the Chern number of pocket  $10_2$  vanishes as it now encloses two WPs of opposite chirality. The two WPs merge together and annihilate at  $\phi \simeq 50^\circ$ .

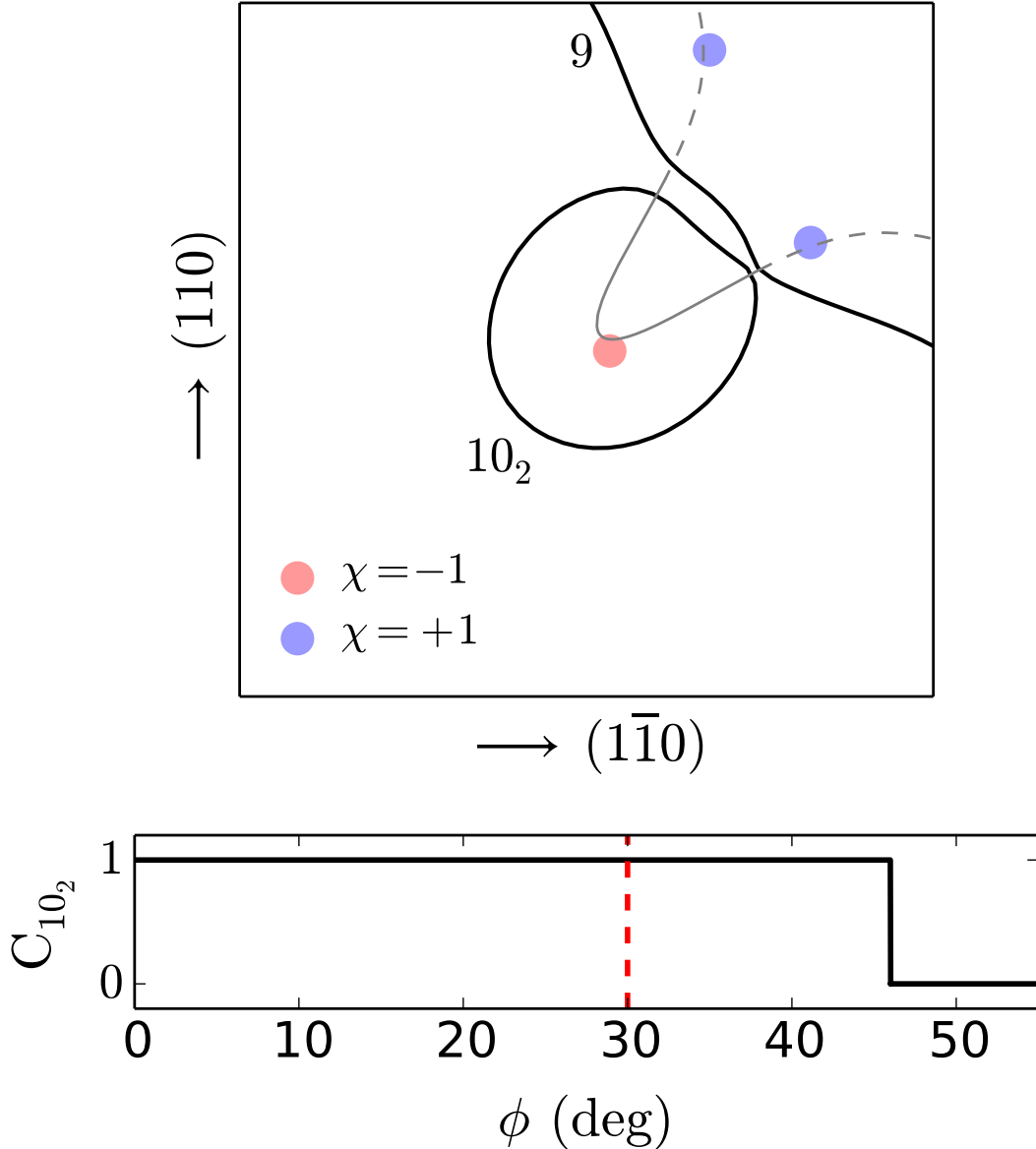


FIG. S7. Upper panel: Fermi contours of bands nine and ten, calculated with the magnetization tilted by  $20^\circ$  (the azimuthal angle  $\phi$  is indicated by the dashed red line in the lower panel). The remnant Weyl points are displayed as colored disks, and the evaporated nodal ring is shown as a guide to the eye. Lower panel: Chern number of pocket  $10_2$  versus  $\phi$ .

The series of snapshots in Figs. S3-S19 depict the evolution of sheets 9 and  $10_2$ , and the motion of nearby remanant Weyl points (WPs), as the tilted magnetization precesses around [001] ( $\phi$  is the azimuthal precession angle). In order to see clearly the touching event between the two sheets at  $\phi \simeq 46^\circ$ , the Fermi contours are not drawn at exactly  $k_z = 0$ : in each snapshot the  $k_z$  coordinate of the contours is pinned to the WP that joins the two sheets at the critical angle (in practice  $k_z$  varies only slightly from one snapshot to the next, never deviating by more than  $0.004 \times 2\pi/a$  from  $k_z = 0$ ). The touching event at  $\phi \simeq 46^\circ$  leads to a transfer of Chern number between the two sheets, after which the Chern number of pocket  $10_2$  vanishes as it now encloses two WPs of opposite chirality. The two WPs merge together and annihilate at  $\phi \simeq 50^\circ$ .

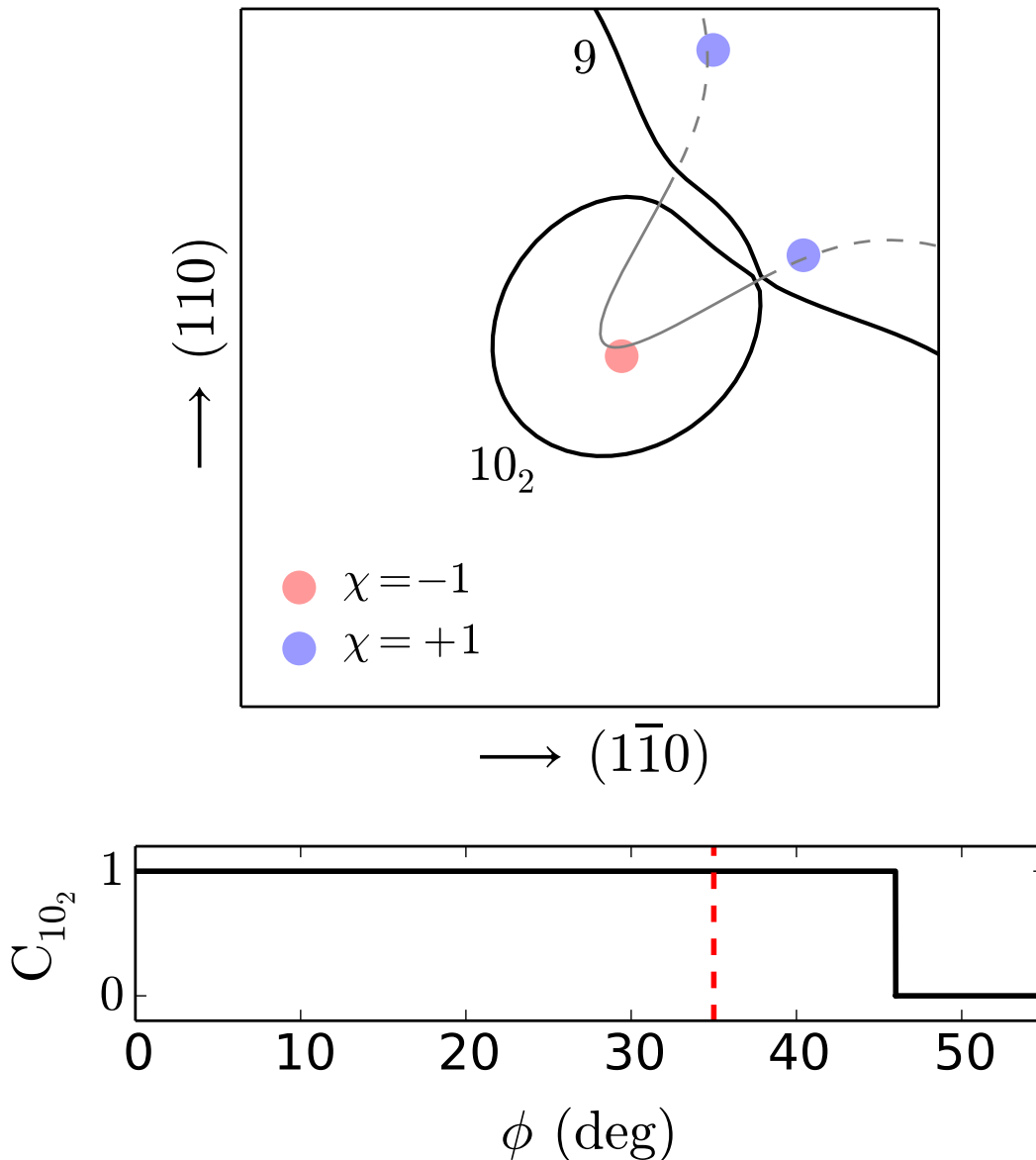


FIG. S8. Upper panel: Fermi contours of bands nine and ten, calculated with the magnetization tilted by  $20^\circ$  (the azimuthal angle  $\phi$  is indicated by the dashed red line in the lower panel). The remnant Weyl points are displayed as colored disks, and the evaporated nodal ring is shown as a guide to the eye. Lower panel: Chern number of pocket  $10_2$  versus  $\phi$ .



The series of snapshots in Figs. S3-S19 depict the evolution of sheets 9 and  $10_2$ , and the motion of nearby remanant Weyl points (WPs), as the tilted magnetization precesses around  $[001]$  ( $\phi$  is the azimuthal precession angle). In order to see clearly the touching event between the two sheets at  $\phi \simeq 46^\circ$ , the Fermi contours are not drawn at exactly  $k_z = 0$ : in each snapshot the  $k_z$  coordinate of the contours is pinned to the WP that joins the two sheets at the critical angle (in practice  $k_z$  varies only slightly from one snapshot to the next, never deviating by more than  $0.004 \times 2\pi/a$  from  $k_z = 0$ ). The touching event at  $\phi \simeq 46^\circ$  leads to a transfer of Chern number between the two sheets, after which the Chern number of pocket  $10_2$  vanishes as it now encloses two WPs of opposite chirality. The two WPs merge together and annihilate at  $\phi \simeq 50^\circ$ .

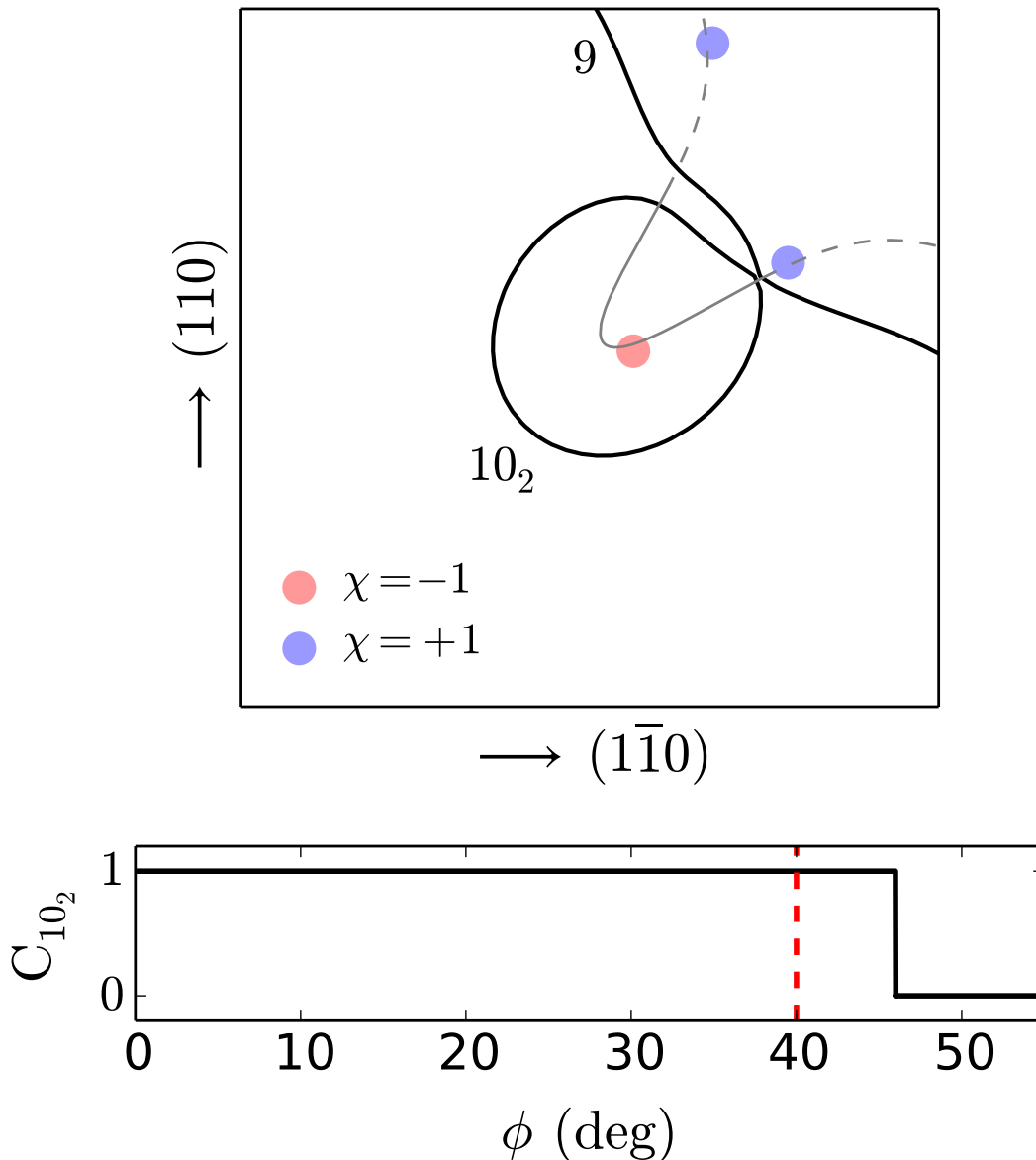


FIG. S9. Upper panel: Fermi contours of bands nine and ten, calculated with the magnetization tilted by  $20^\circ$  (the azimuthal angle  $\phi$  is indicated by the dashed red line in the lower panel). The remnant Weyl points are displayed as colored disks, and the evaporated nodal ring is shown as a guide to the eye. Lower panel: Chern number of pocket  $10_2$  versus  $\phi$ .

The series of snapshots in Figs. S3-S19 depict the evolution of sheets 9 and  $10_2$ , and the motion of nearby remanant Weyl points (WPs), as the tilted magnetization precesses around  $[001]$  ( $\phi$  is the azimuthal precession angle). In order to see clearly the touching event between the two sheets at  $\phi \simeq 46^\circ$ , the Fermi contours are not drawn at exactly  $k_z = 0$ : in each snapshot the  $k_z$  coordinate of the contours is pinned to the WP that joins the two sheets at the critical angle (in practice  $k_z$  varies only slightly from one snapshot to the next, never deviating by more than  $0.004 \times 2\pi/a$  from  $k_z = 0$ ). The touching event at  $\phi \simeq 46^\circ$  leads to a transfer of Chern number between the two sheets, after which the Chern number of pocket  $10_2$  vanishes as it now encloses two WPs of opposite chirality. The two WPs merge together and annihilate at  $\phi \simeq 50^\circ$ .

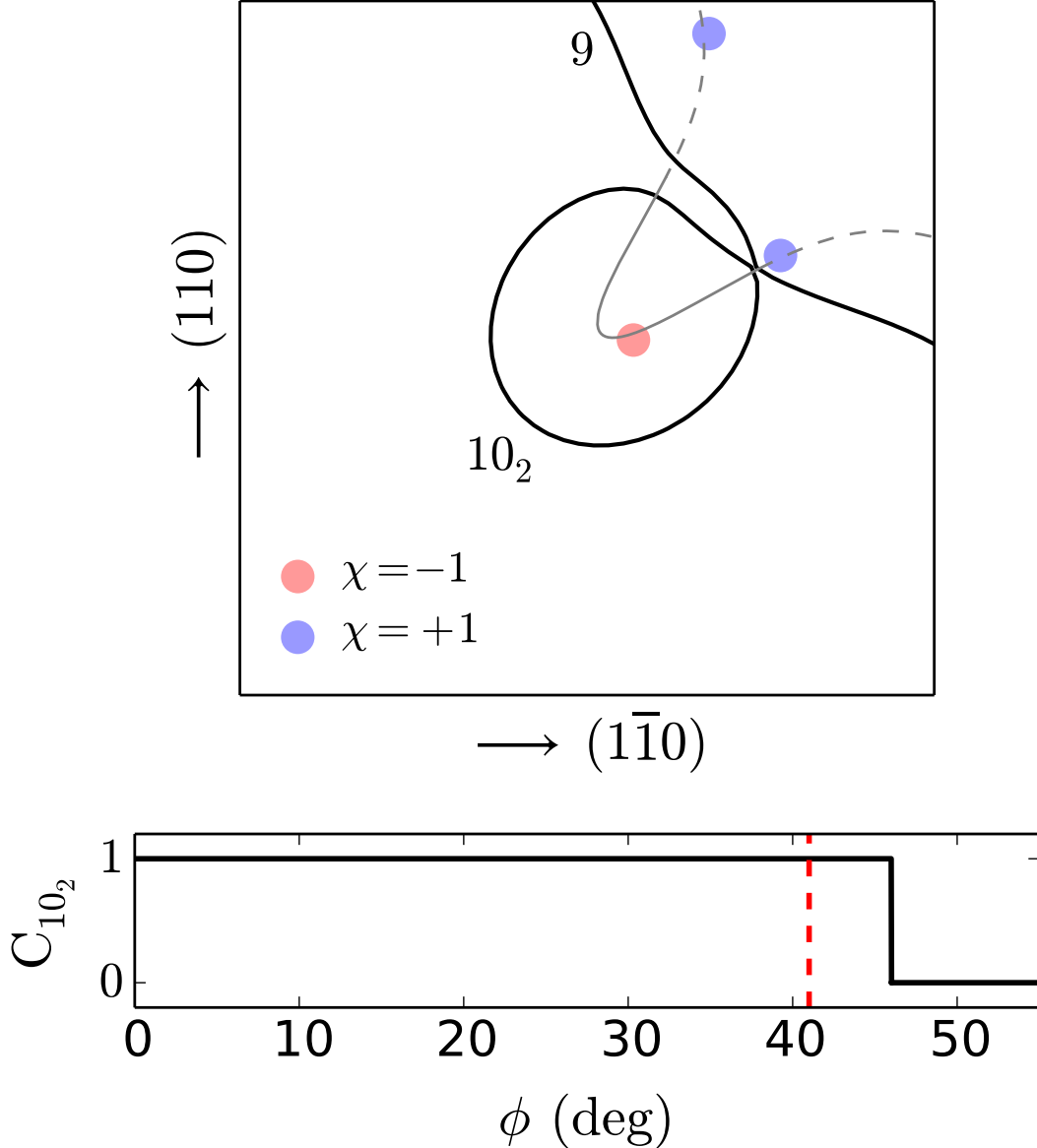


FIG. S10. Upper panel: Fermi contours of bands nine and ten, calculated with the magnetization tilted by  $20^\circ$  (the azimuthal angle  $\phi$  is indicated by the dashed red line in the lower panel). The remnant Weyl points are displayed as colored disks, and the evaporated nodal ring is shown as a guide to the eye. Lower panel: Chern number of pocket  $10_2$  versus  $\phi$ .

The series of snapshots in Figs. S3-S19 depict the evolution of sheets 9 and  $10_2$ , and the motion of nearby remanant Weyl points (WPs), as the tilted magnetization precesses around  $[001]$  ( $\phi$  is the azimuthal precession angle). In order to see clearly the touching event between the two sheets at  $\phi \simeq 46^\circ$ , the Fermi contours are not drawn at exactly  $k_z = 0$ : in each snapshot the  $k_z$  coordinate of the contours is pinned to the WP that joins the two sheets at the critical angle (in practice  $k_z$  varies only slightly from one snapshot to the next, never deviating by more than  $0.004 \times 2\pi/a$  from  $k_z = 0$ ). The touching event at  $\phi \simeq 46^\circ$  leads to a transfer of Chern number between the two sheets, after which the Chern number of pocket  $10_2$  vanishes as it now encloses two WPs of opposite chirality. The two WPs merge together and annihilate at  $\phi \simeq 50^\circ$ .

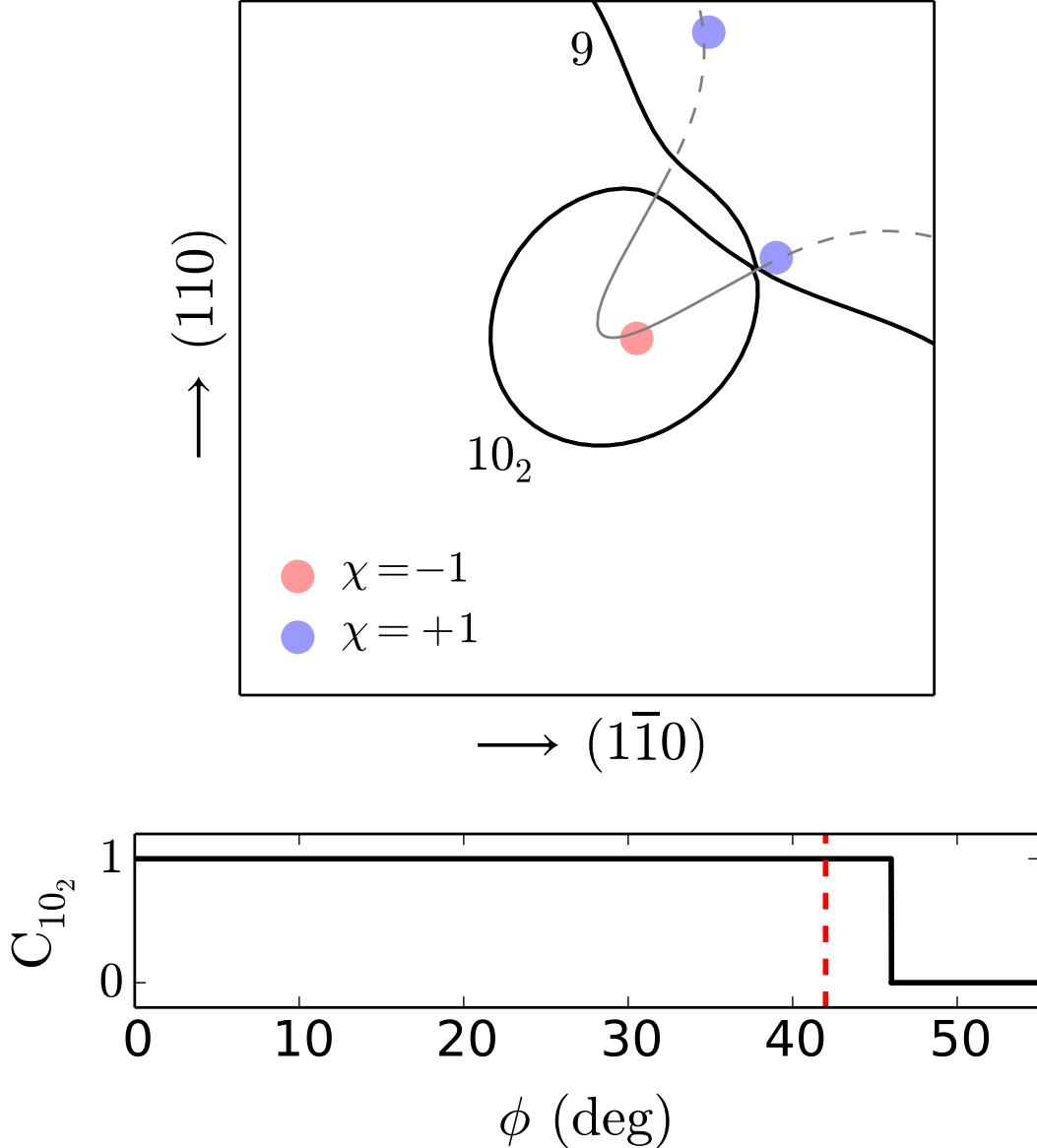


FIG. S11. Upper panel: Fermi contours of bands nine and ten, calculated with the magnetization tilted by  $20^\circ$  (the azimuthal angle  $\phi$  is indicated by the dashed red line in the lower panel). The remnant Weyl points are displayed as colored disks, and the evaporated nodal ring is shown as a guide to the eye. Lower panel: Chern number of pocket  $10_2$  versus  $\phi$ .

The series of snapshots in Figs. S3-S19 depict the evolution of sheets 9 and  $10_2$ , and the motion of nearby remanant Weyl points (WPs), as the tilted magnetization precesses around  $[001]$  ( $\phi$  is the azimuthal precession angle). In order to see clearly the touching event between the two sheets at  $\phi \simeq 46^\circ$ , the Fermi contours are not drawn at exactly  $k_z = 0$ : in each snapshot the  $k_z$  coordinate of the contours is pinned to the WP that joins the two sheets at the critical angle (in practice  $k_z$  varies only slightly from one snapshot to the next, never deviating by more than  $0.004 \times 2\pi/a$  from  $k_z = 0$ ). The touching event at  $\phi \simeq 46^\circ$  leads to a transfer of Chern number between the two sheets, after which the Chern number of pocket  $10_2$  vanishes as it now encloses two WPs of opposite chirality. The two WPs merge together and annihilate at  $\phi \simeq 50^\circ$ .

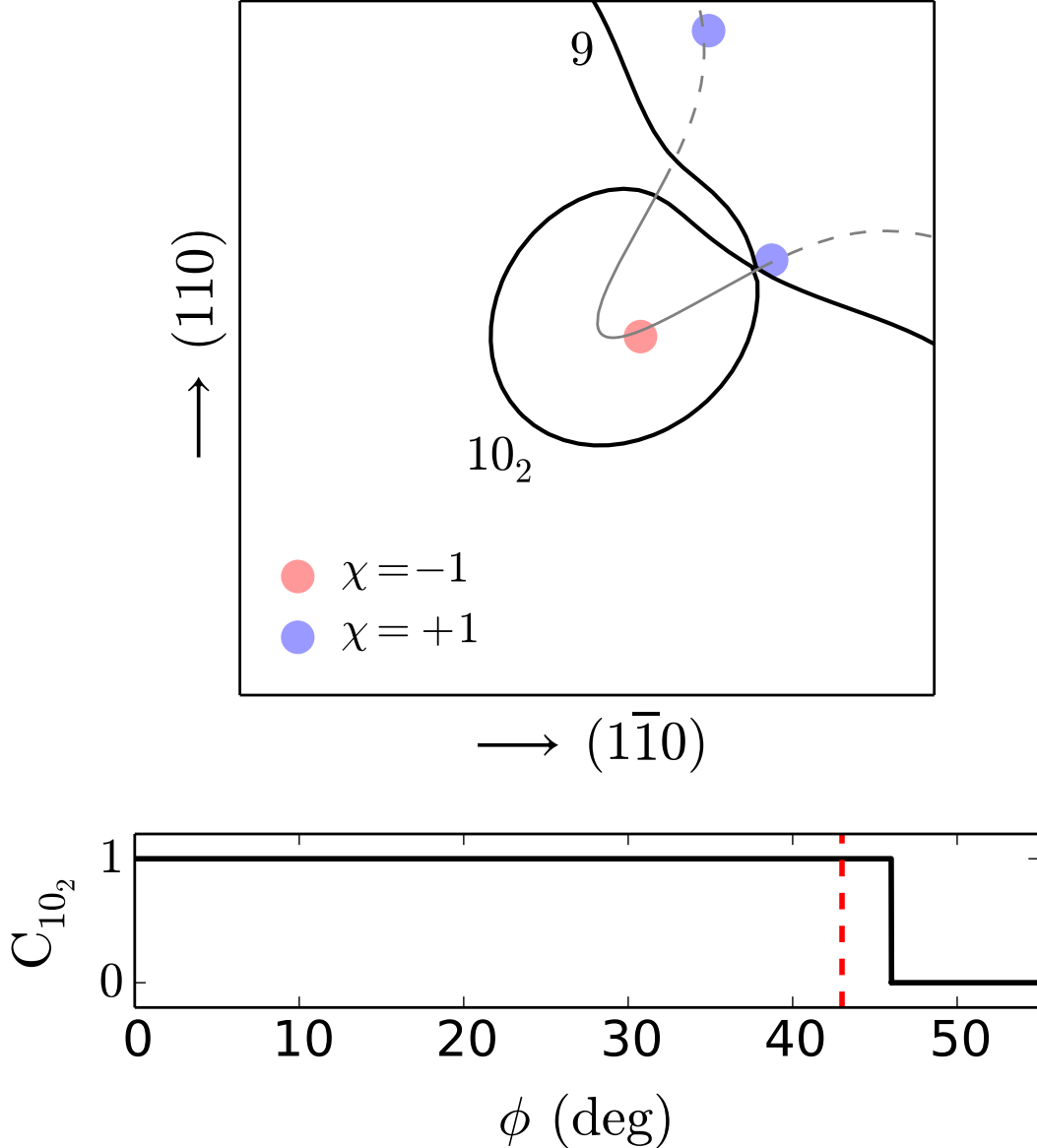


FIG. S12. Upper panel: Fermi contours of bands nine and ten, calculated with the magnetization tilted by  $20^\circ$  (the azimuthal angle  $\phi$  is indicated by the dashed red line in the lower panel). The remnant Weyl points are displayed as colored disks, and the evaporated nodal ring is shown as a guide to the eye. Lower panel: Chern number of pocket  $10_2$  versus  $\phi$ .

The series of snapshots in Figs. S3-S19 depict the evolution of sheets 9 and  $10_2$ , and the motion of nearby remanant Weyl points (WPs), as the tilted magnetization precesses around  $[001]$  ( $\phi$  is the azimuthal precession angle). In order to see clearly the touching event between the two sheets at  $\phi \simeq 46^\circ$ , the Fermi contours are not drawn at exactly  $k_z = 0$ : in each snapshot the  $k_z$  coordinate of the contours is pinned to the WP that joins the two sheets at the critical angle (in practice  $k_z$  varies only slightly from one snapshot to the next, never deviating by more than  $0.004 \times 2\pi/a$  from  $k_z = 0$ ). The touching event at  $\phi \simeq 46^\circ$  leads to a transfer of Chern number between the two sheets, after which the Chern number of pocket  $10_2$  vanishes as it now encloses two WPs of opposite chirality. The two WPs merge together and annihilate at  $\phi \simeq 50^\circ$ .

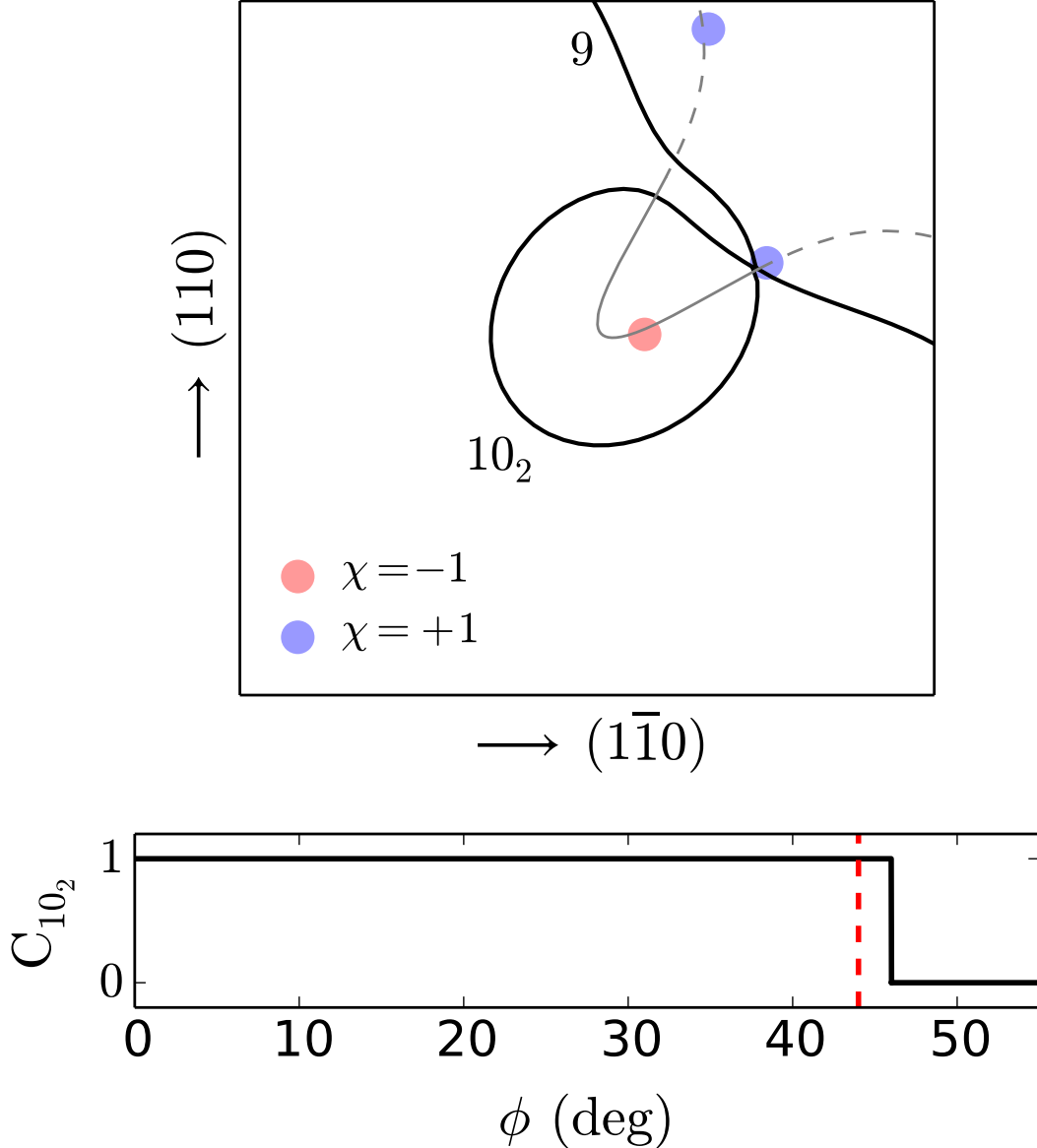


FIG. S13. Upper panel: Fermi contours of bands nine and ten, calculated with the magnetization tilted by  $20^\circ$  (the azimuthal angle  $\phi$  is indicated by the dashed red line in the lower panel). The remnant Weyl points are displayed as colored disks, and the evaporated nodal ring is shown as a guide to the eye. Lower panel: Chern number of pocket  $10_2$  versus  $\phi$ .

The series of snapshots in Figs. S3-S19 depict the evolution of sheets 9 and  $10_2$ , and the motion of nearby remanant Weyl points (WPs), as the tilted magnetization precesses around  $[001]$  ( $\phi$  is the azimuthal precession angle). In order to see clearly the touching event between the two sheets at  $\phi \simeq 46^\circ$ , the Fermi contours are not drawn at exactly  $k_z = 0$ : in each snapshot the  $k_z$  coordinate of the contours is pinned to the WP that joins the two sheets at the critical angle (in practice  $k_z$  varies only slightly from one snapshot to the next, never deviating by more than  $0.004 \times 2\pi/a$  from  $k_z = 0$ ). The touching event at  $\phi \simeq 46^\circ$  leads to a transfer of Chern number between the two sheets, after which the Chern number of pocket  $10_2$  vanishes as it now encloses two WPs of opposite chirality. The two WPs merge together and annihilate at  $\phi \simeq 50^\circ$ .

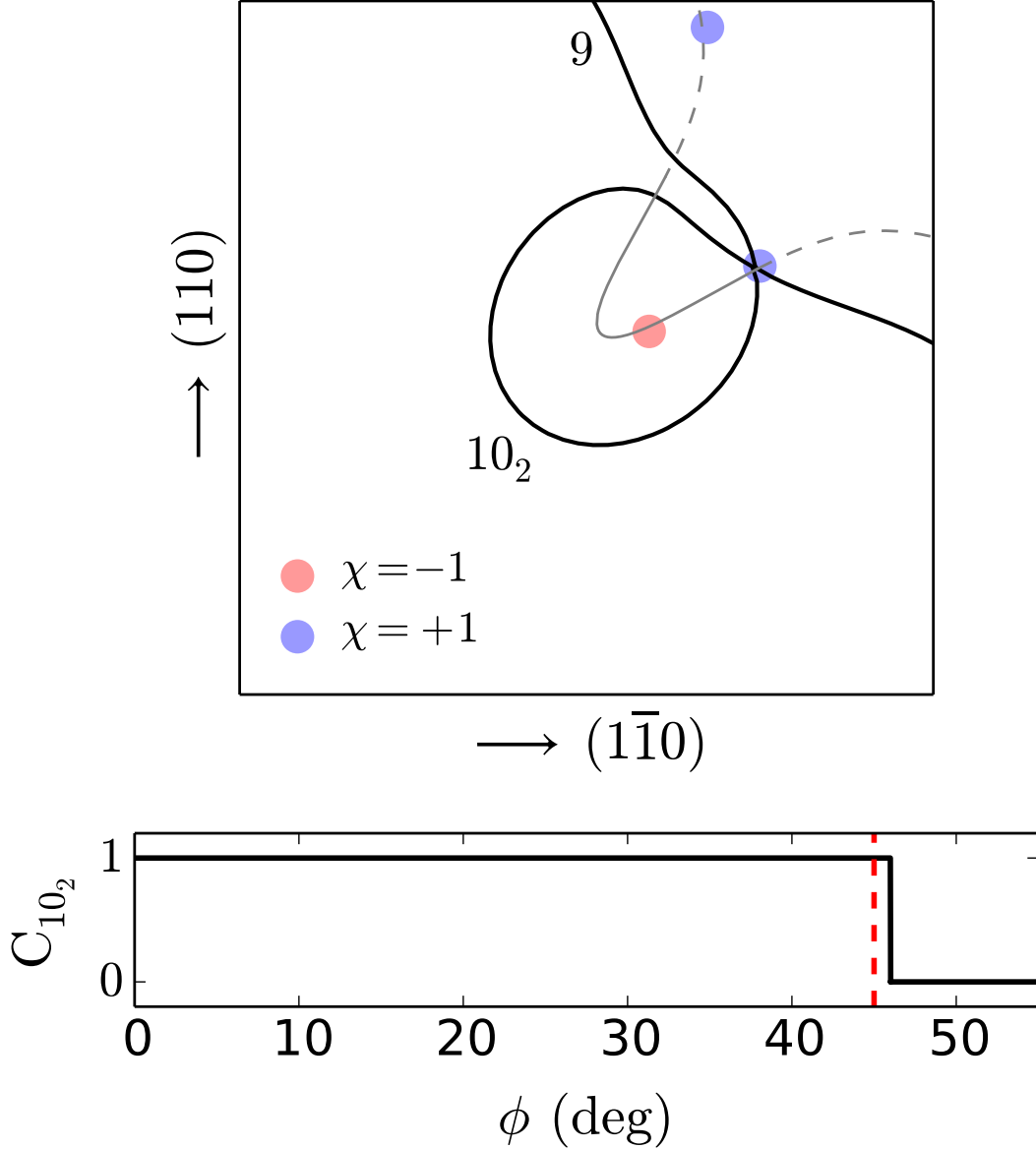


FIG. S14. Upper panel: Fermi contours of bands nine and ten, calculated with the magnetization tilted by  $20^\circ$  (the azimuthal angle  $\phi$  is indicated by the dashed red line in the lower panel). The remnant Weyl points are displayed as colored disks, and the evaporated nodal ring is shown as a guide to the eye. Lower panel: Chern number of pocket  $10_2$  versus  $\phi$ .

The series of snapshots in Figs. S3-S19 depict the evolution of sheets 9 and  $10_2$ , and the motion of nearby remanant Weyl points (WPs), as the tilted magnetization precesses around  $[001]$  ( $\phi$  is the azimuthal precession angle). In order to see clearly the touching event between the two sheets at  $\phi \simeq 46^\circ$ , the Fermi contours are not drawn at exactly  $k_z = 0$ : in each snapshot the  $k_z$  coordinate of the contours is pinned to the WP that joins the two sheets at the critical angle (in practice  $k_z$  varies only slightly from one snapshot to the next, never deviating by more than  $0.004 \times 2\pi/a$  from  $k_z = 0$ ). The touching event at  $\phi \simeq 46^\circ$  leads to a transfer of Chern number between the two sheets, after which the Chern number of pocket  $10_2$  vanishes as it now encloses two WPs of opposite chirality. The two WPs merge together and annihilate at  $\phi \simeq 50^\circ$ .

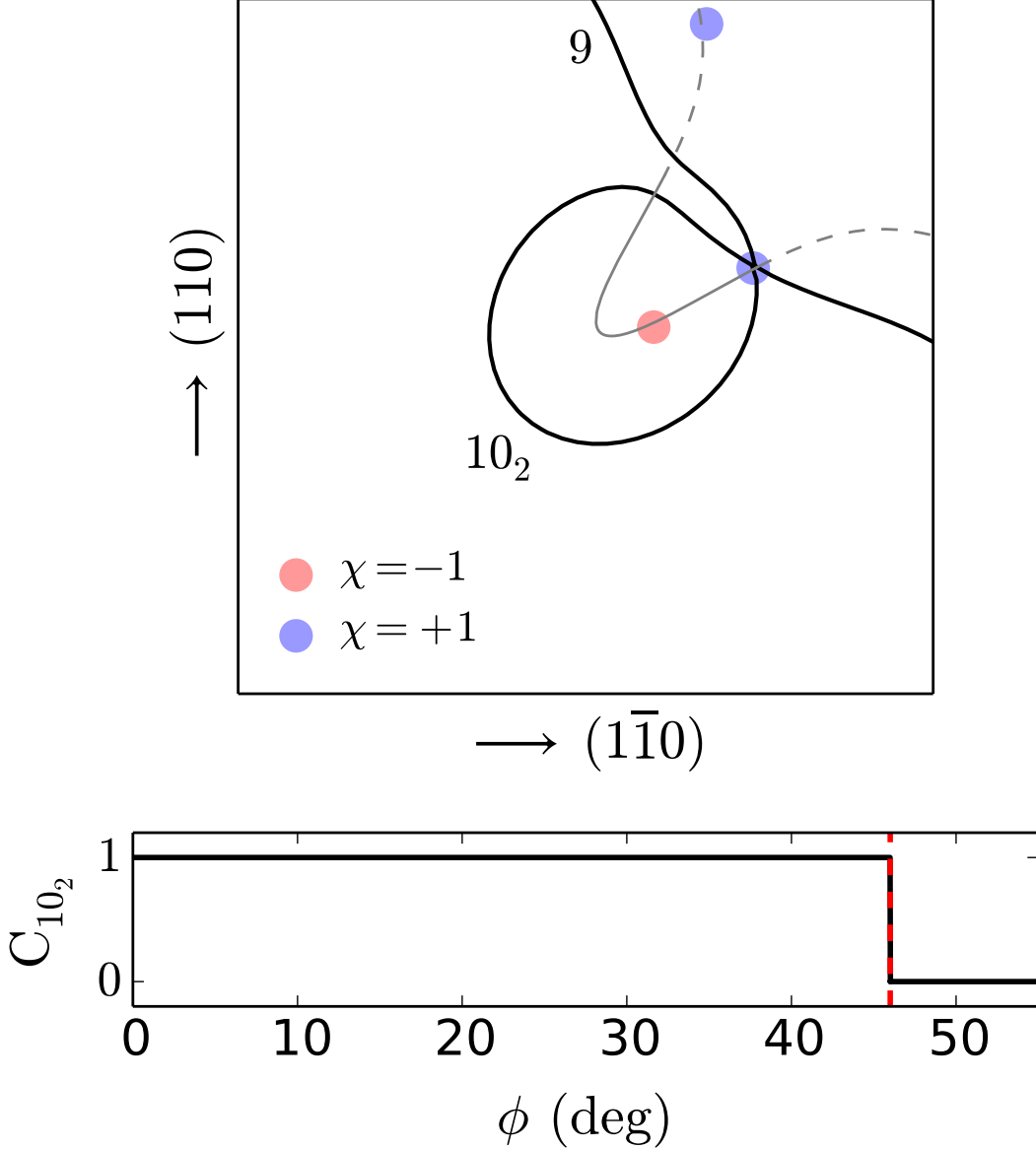


FIG. S15. Upper panel: Fermi contours of bands nine and ten, calculated with the magnetization tilted by  $20^\circ$  (the azimuthal angle  $\phi$  is indicated by the dashed red line in the lower panel). The remnant Weyl points are displayed as colored disks, and the evaporated nodal ring is shown as a guide to the eye. Lower panel: Chern number of pocket  $10_2$  versus  $\phi$ .

The series of snapshots in Figs. S3-S19 depict the evolution of sheets 9 and  $10_2$ , and the motion of nearby remanant Weyl points (WPs), as the tilted magnetization precesses around  $[001]$  ( $\phi$  is the azimuthal precession angle). In order to see clearly the touching event between the two sheets at  $\phi \simeq 46^\circ$ , the Fermi contours are not drawn at exactly  $k_z = 0$ : in each snapshot the  $k_z$  coordinate of the contours is pinned to the WP that joins the two sheets at the critical angle (in practice  $k_z$  varies only slightly from one snapshot to the next, never deviating by more than  $0.004 \times 2\pi/a$  from  $k_z = 0$ ). The touching event at  $\phi \simeq 46^\circ$  leads to a transfer of Chern number between the two sheets, after which the Chern number of pocket  $10_2$  vanishes as it now encloses two WPs of opposite chirality. The two WPs merge together and annihilate at  $\phi \simeq 50^\circ$ .

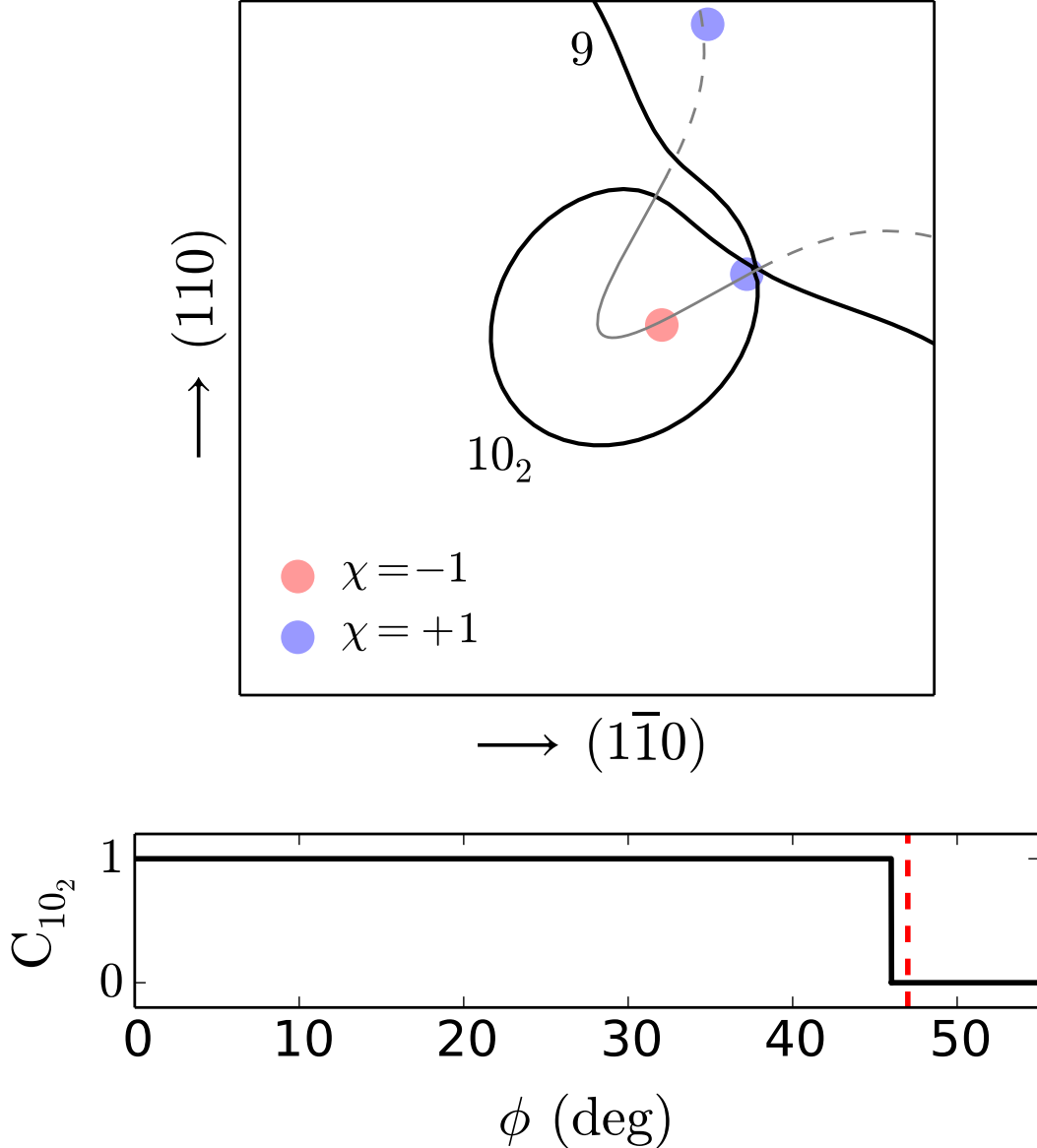


FIG. S16. Upper panel: Fermi contours of bands nine and ten, calculated with the magnetization tilted by  $20^\circ$  (the azimuthal angle  $\phi$  is indicated by the dashed red line in the lower panel). The remnant Weyl points are displayed as colored disks, and the evaporated nodal ring is shown as a guide to the eye. Lower panel: Chern number of pocket  $10_2$  versus  $\phi$ .



The series of snapshots in Figs. S3-S19 depict the evolution of sheets 9 and  $10_2$ , and the motion of nearby remanant Weyl points (WPs), as the tilted magnetization precesses around  $[001]$  ( $\phi$  is the azimuthal precession angle). In order to see clearly the touching event between the two sheets at  $\phi \simeq 46^\circ$ , the Fermi contours are not drawn at exactly  $k_z = 0$ : in each snapshot the  $k_z$  coordinate of the contours is pinned to the WP that joins the two sheets at the critical angle (in practice  $k_z$  varies only slightly from one snapshot to the next, never deviating by more than  $0.004 \times 2\pi/a$  from  $k_z = 0$ ). The touching event at  $\phi \simeq 46^\circ$  leads to a transfer of Chern number between the two sheets, after which the Chern number of pocket  $10_2$  vanishes as it now encloses two WPs of opposite chirality. The two WPs merge together and annihilate at  $\phi \simeq 50^\circ$ .

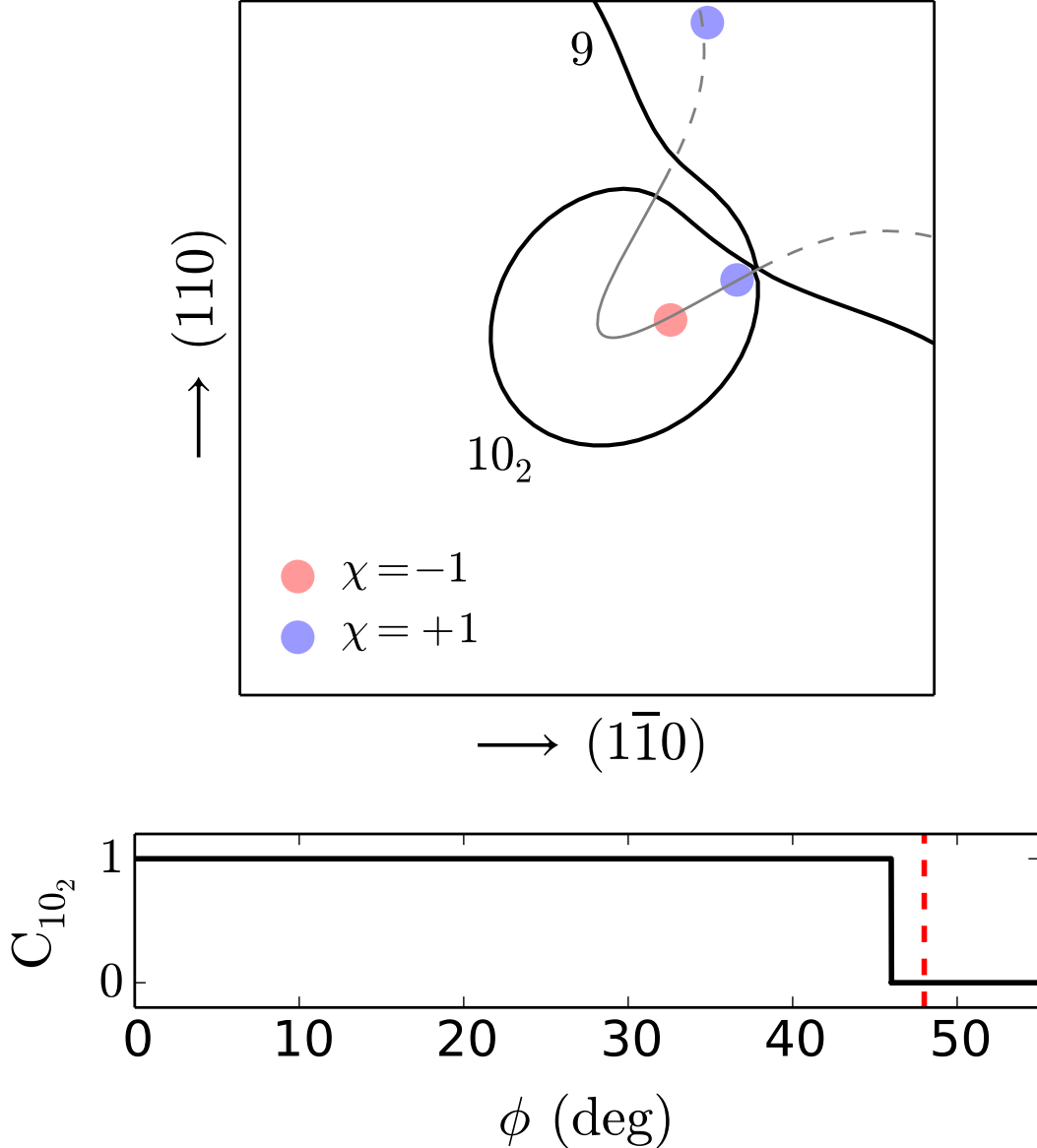


FIG. S17. Upper panel: Fermi contours of bands nine and ten, calculated with the magnetization tilted by  $20^\circ$  (the azimuthal angle  $\phi$  is indicated by the dashed red line in the lower panel). The remnant Weyl points are displayed as colored disks, and the evaporated nodal ring is shown as a guide to the eye. Lower panel: Chern number of pocket  $10_2$  versus  $\phi$ .

The series of snapshots in Figs. S3-S19 depict the evolution of sheets 9 and  $10_2$ , and the motion of nearby remanant Weyl points (WPs), as the tilted magnetization precesses around  $[001]$  ( $\phi$  is the azimuthal precession angle). In order to see clearly the touching event between the two sheets at  $\phi \simeq 46^\circ$ , the Fermi contours are not drawn at exactly  $k_z = 0$ : in each snapshot the  $k_z$  coordinate of the contours is pinned to the WP that joins the two sheets at the critical angle (in practice  $k_z$  varies only slightly from one snapshot to the next, never deviating by more than  $0.004 \times 2\pi/a$  from  $k_z = 0$ ). The touching event at  $\phi \simeq 46^\circ$  leads to a transfer of Chern number between the two sheets, after which the Chern number of pocket  $10_2$  vanishes as it now encloses two WPs of opposite chirality. The two WPs merge together and annihilate at  $\phi \simeq 50^\circ$ .

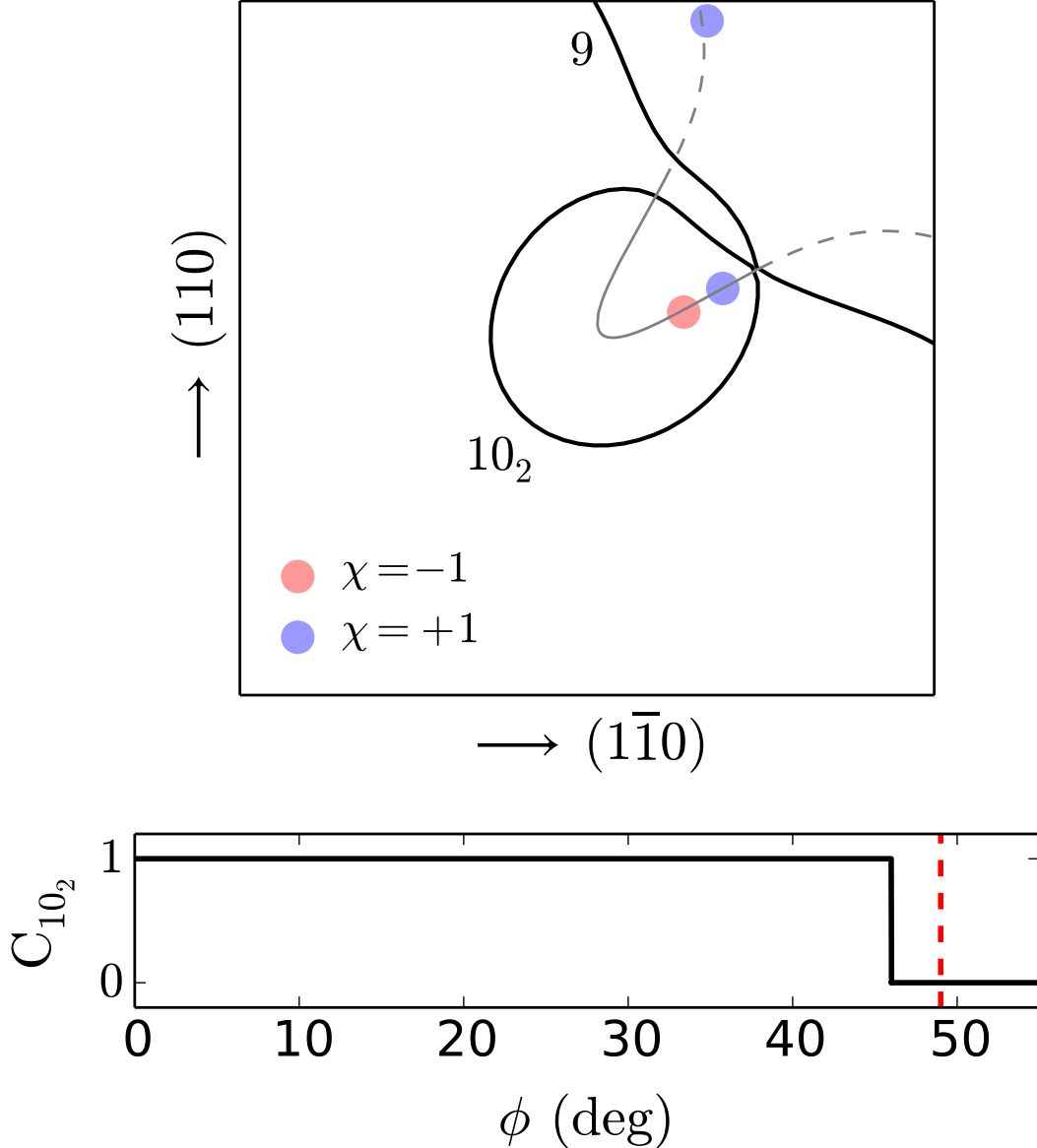


FIG. S18. Upper panel: Fermi contours of bands nine and ten, calculated with the magnetization tilted by  $20^\circ$  (the azimuthal angle  $\phi$  is indicated by the dashed red line in the lower panel). The remnant Weyl points are displayed as colored disks, and the evaporated nodal ring is shown as a guide to the eye. Lower panel: Chern number of pocket  $10_2$  versus  $\phi$ .

The series of snapshots in Figs. S3-S19 depict the evolution of sheets 9 and  $10_2$ , and the motion of nearby remanant Weyl points (WPs), as the tilted magnetization precesses around  $[001]$  ( $\phi$  is the azimuthal precession angle). In order to see clearly the touching event between the two sheets at  $\phi \simeq 46^\circ$ , the Fermi contours are not drawn at exactly  $k_z = 0$ : in each snapshot the  $k_z$  coordinate of the contours is pinned to the WP that joins the two sheets at the critical angle (in practice  $k_z$  varies only slightly from one snapshot to the next, never deviating by more than  $0.004 \times 2\pi/a$  from  $k_z = 0$ ). The touching event at  $\phi \simeq 46^\circ$  leads to a transfer of Chern number between the two sheets, after which the Chern number of pocket  $10_2$  vanishes as it now encloses two WPs of opposite chirality. The two WPs merge together and annihilate at  $\phi \simeq 50^\circ$ .

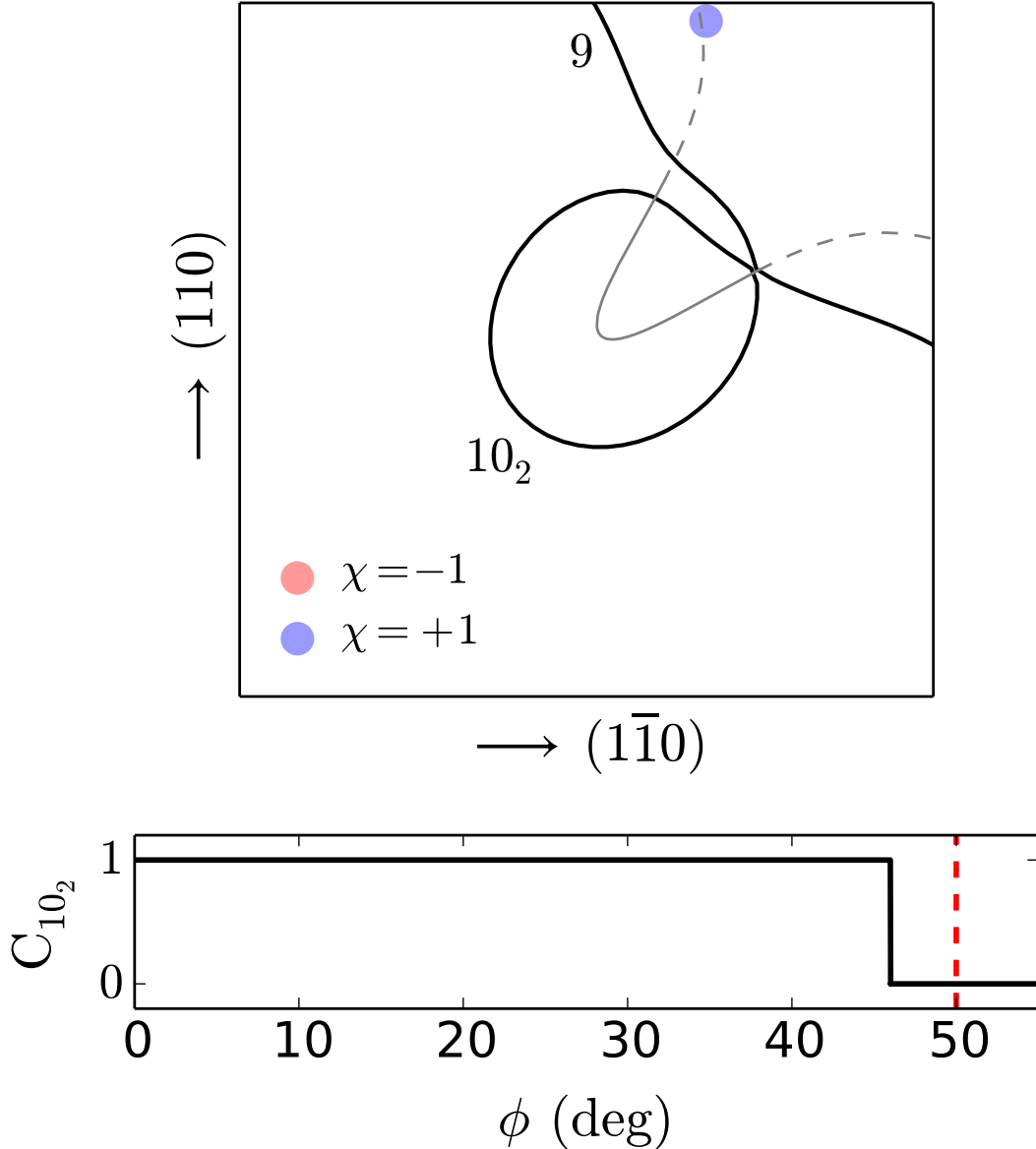


FIG. S19. Upper panel: Fermi contours of bands nine and ten, calculated with the magnetization tilted by  $20^\circ$  (the azimuthal angle  $\phi$  is indicated by the dashed red line in the lower panel). The remnant Weyl points are displayed as colored disks, and the evaporated nodal ring is shown as a guide to the eye. Lower panel: Chern number of pocket  $10_2$  versus  $\phi$ .

## II. CHIRAL TOUCHING BETWEEN FERMI SHEETS UPON VARYING THE FERMI LEVEL

All the calculations presented in this section were done with the magnetization pointing along the easy axis  $[001]$ . Figure S20 shows the Fermi contours of bands nine and ten on the  $\Gamma$ NP ( $k_x = k_y$ ) plane in Fig. 3. Pockets 9 and  $10_1$  have zero Chern number, and pockets  $10_6$  and  $10_7$  have Chern numbers  $-1$  and  $+1$  (see Table III). The series of snapshots in Figs. S21-S25 depict the touching event between sheets 9 and  $10_7$  upon increasing the Fermi level, leading to a transfer of Chern number between them (Sec. VI.C.2).

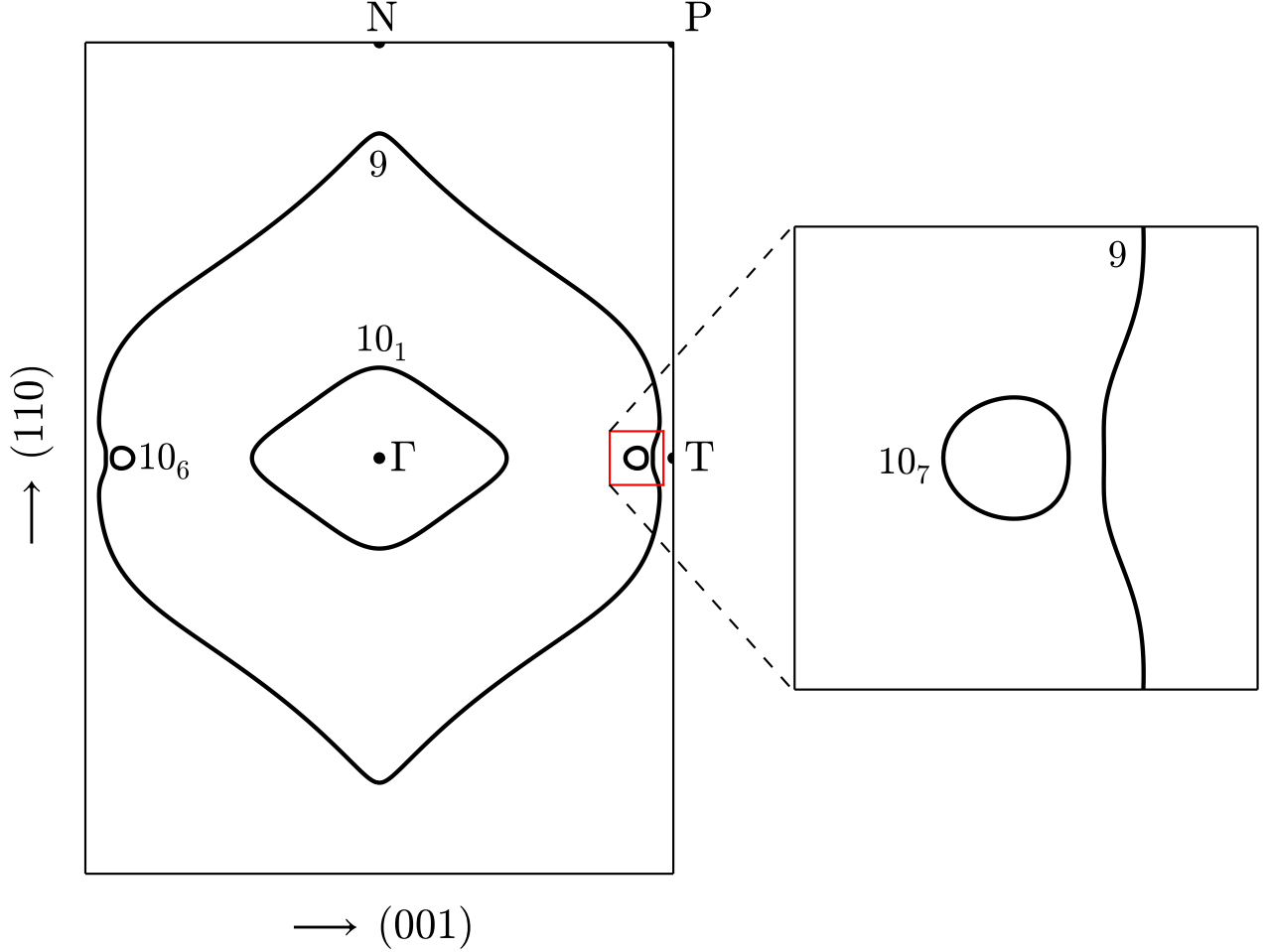


FIG. S20. Left: Fermi contours of bands nine and ten on the  $\Gamma$ NP Brillouin-zone slice at  $k_x = k_y$ , evaluated for the true (unshifted) Fermi level. Right: Detail showing the region of closest approach between sheets 9 and  $10_7$ .

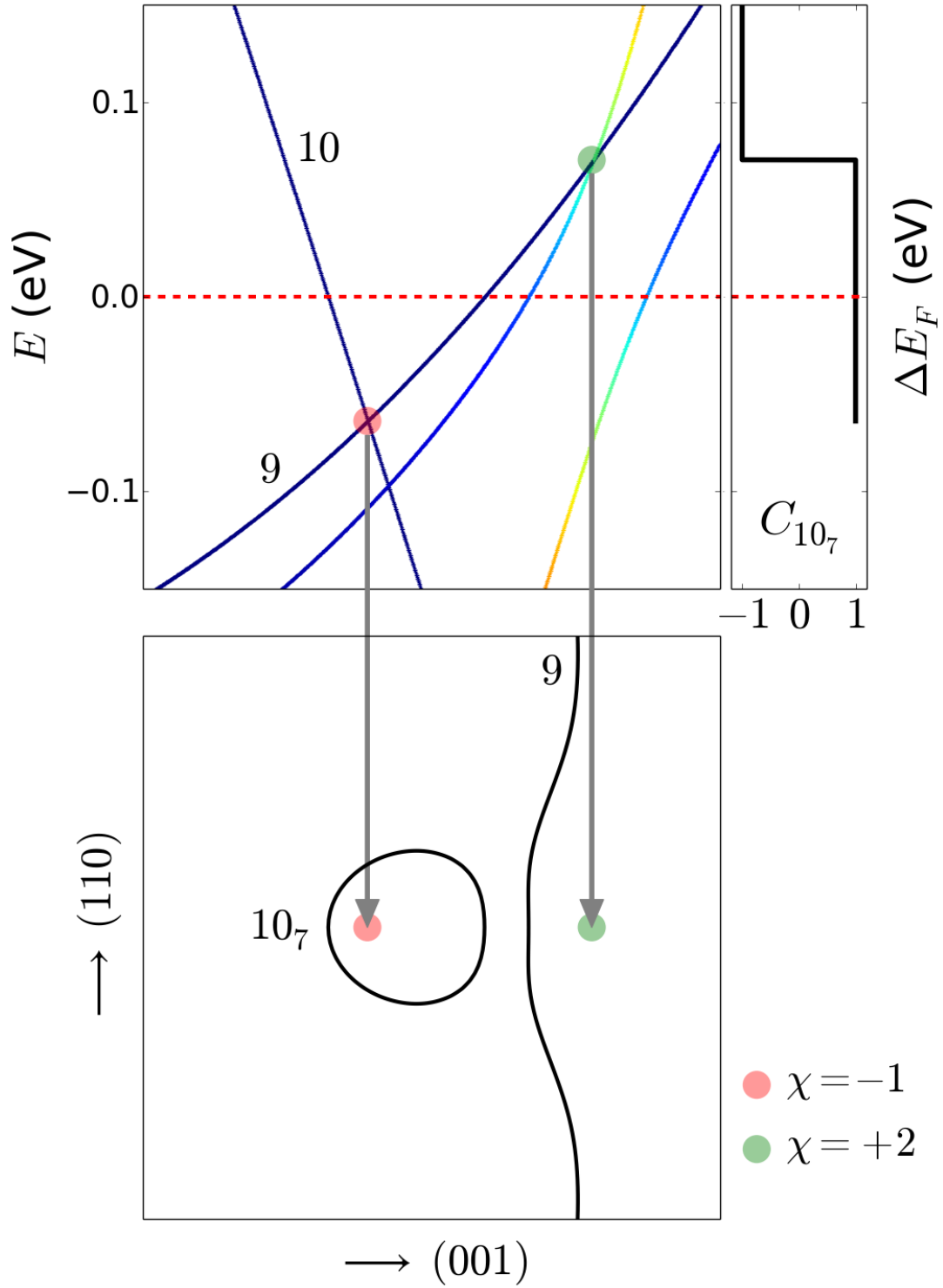


FIG. S21. Upper-left panel: Energy bands along the line  $\Delta$  in Fig. 3, close to the electron pocket  $10_7$  [see also Fig. 13(a)]. Energies are measured from the true Fermi level. Upper-right panel: Chern number of pocket  $10_7$  versus the Fermi-level shift. Lower panel: Fermi contours inside the red square in Fig. S20 for  $\Delta E_F = 0.000$  eV (the dashed red line in the upper panels). The red and green disks represent Weyl nodes between bands nine and ten, and  $\chi$  is the chiral charge.

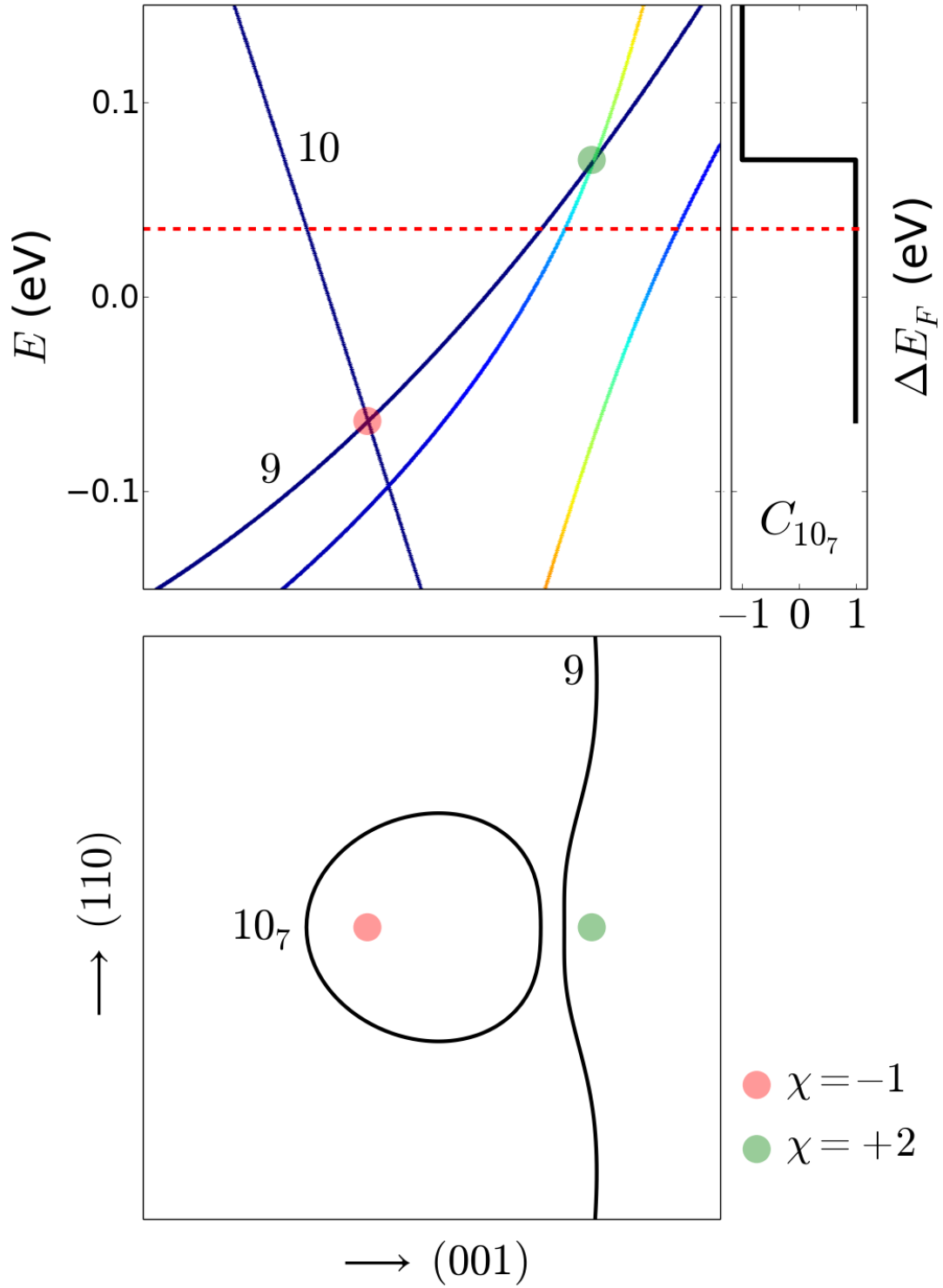


FIG. S22. Upper-left panel: Energy bands along the line  $\Delta$  in Fig. 3, close to the electron pocket  $10_7$  [see also Fig. 13(a)]. Energies are measured from the true Fermi level. Upper-right panel: Chern number of pocket  $10_7$  versus the Fermi-level shift. Lower panel: Fermi contours inside the red square in Fig. S20 for  $\Delta E_F = 0.035$  eV (the dashed red line in the upper panels). The red and green disks represent Weyl nodes between bands nine and ten, and  $\chi$  is the chiral charge.

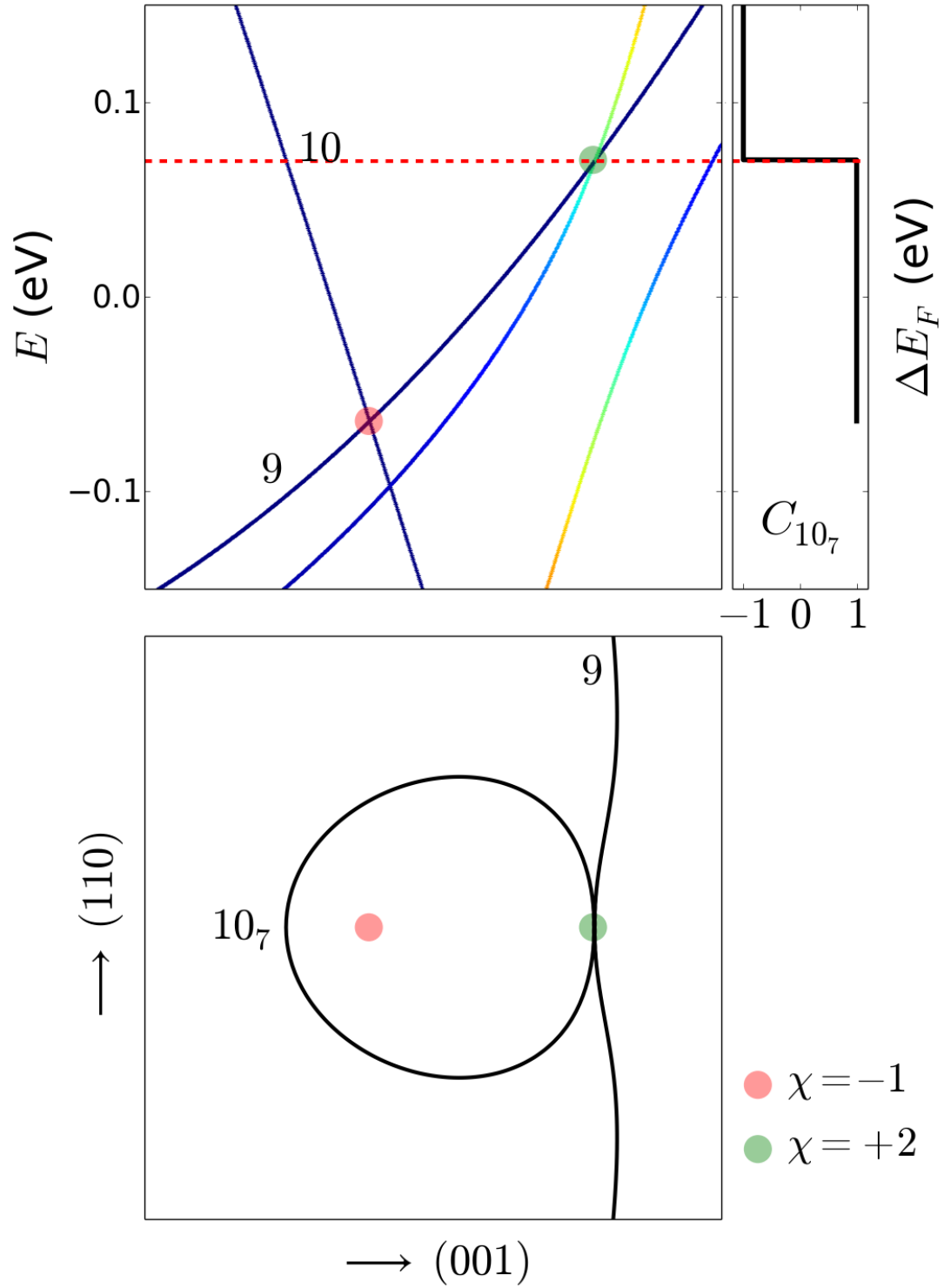


FIG. S23. Upper-left panel: Energy bands along the line  $\Delta$  in Fig. 3, close to the electron pocket  $10_7$  [see also Fig. 13(a)]. Energies are measured from the true Fermi level. Upper-right panel: Chern number of pocket  $10_7$  versus the Fermi-level shift. Lower panel: Fermi contours inside the red square in Fig. S20 for  $\Delta E_F = 0.070$  eV (the dashed red line in the upper panels). The red and green disks represent Weyl nodes between bands nine and ten, and  $\chi$  is the chiral charge.

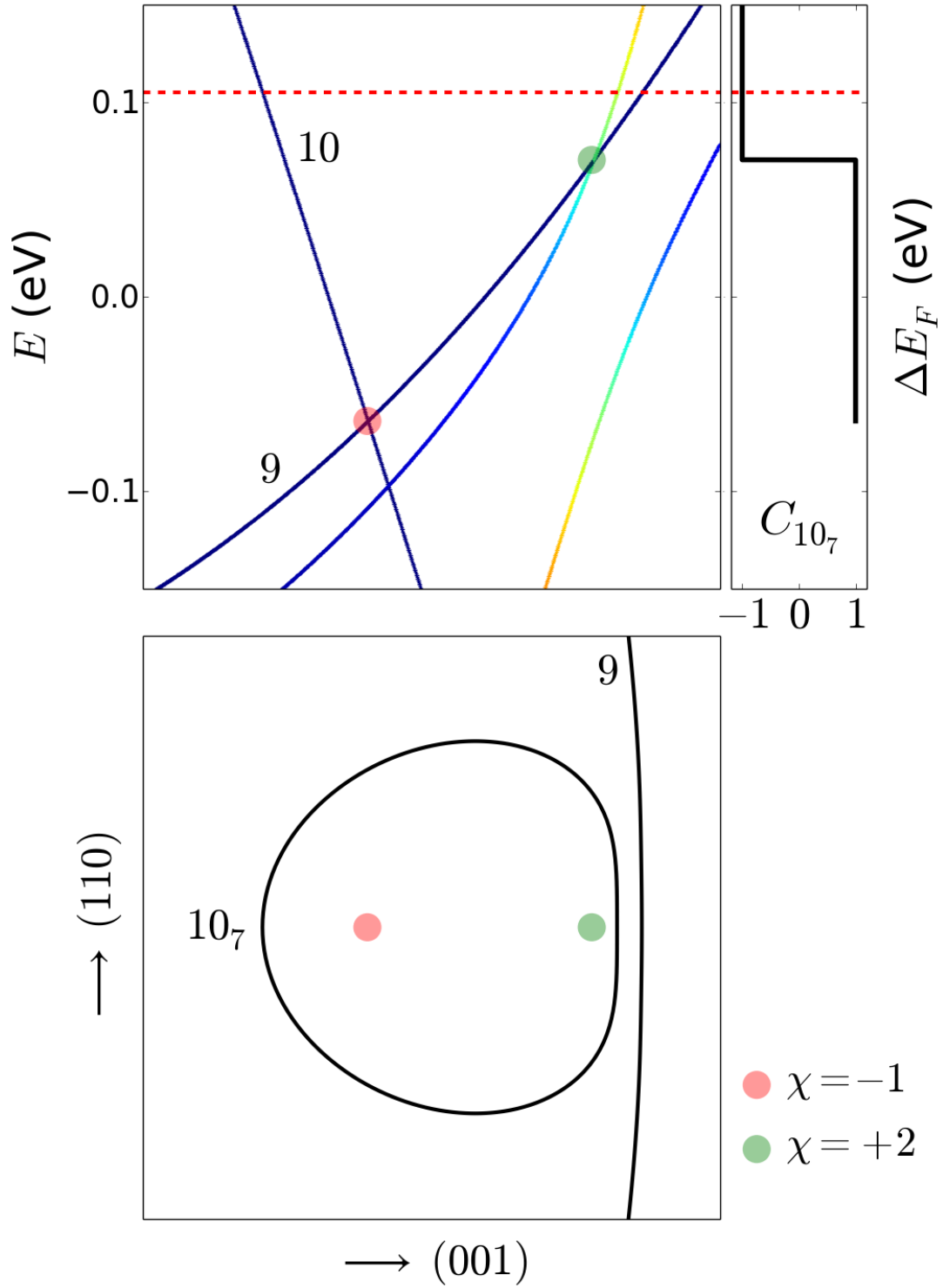


FIG. S24. Upper-left panel: Energy bands along the line  $\Delta$  in Fig. 3, close to the electron pocket  $10_7$  [see also Fig. 13(a)]. Energies are measured from the true Fermi level. Upper-right panel: Chern number of pocket  $10_7$  versus the Fermi-level shift. Lower panel: Fermi contours inside the red square in Fig. S20 for  $\Delta E_F = 0.105$  eV (the dashed red line in the upper panels). The red and green disks represent Weyl nodes between bands nine and ten, and  $\chi$  is the chiral charge.



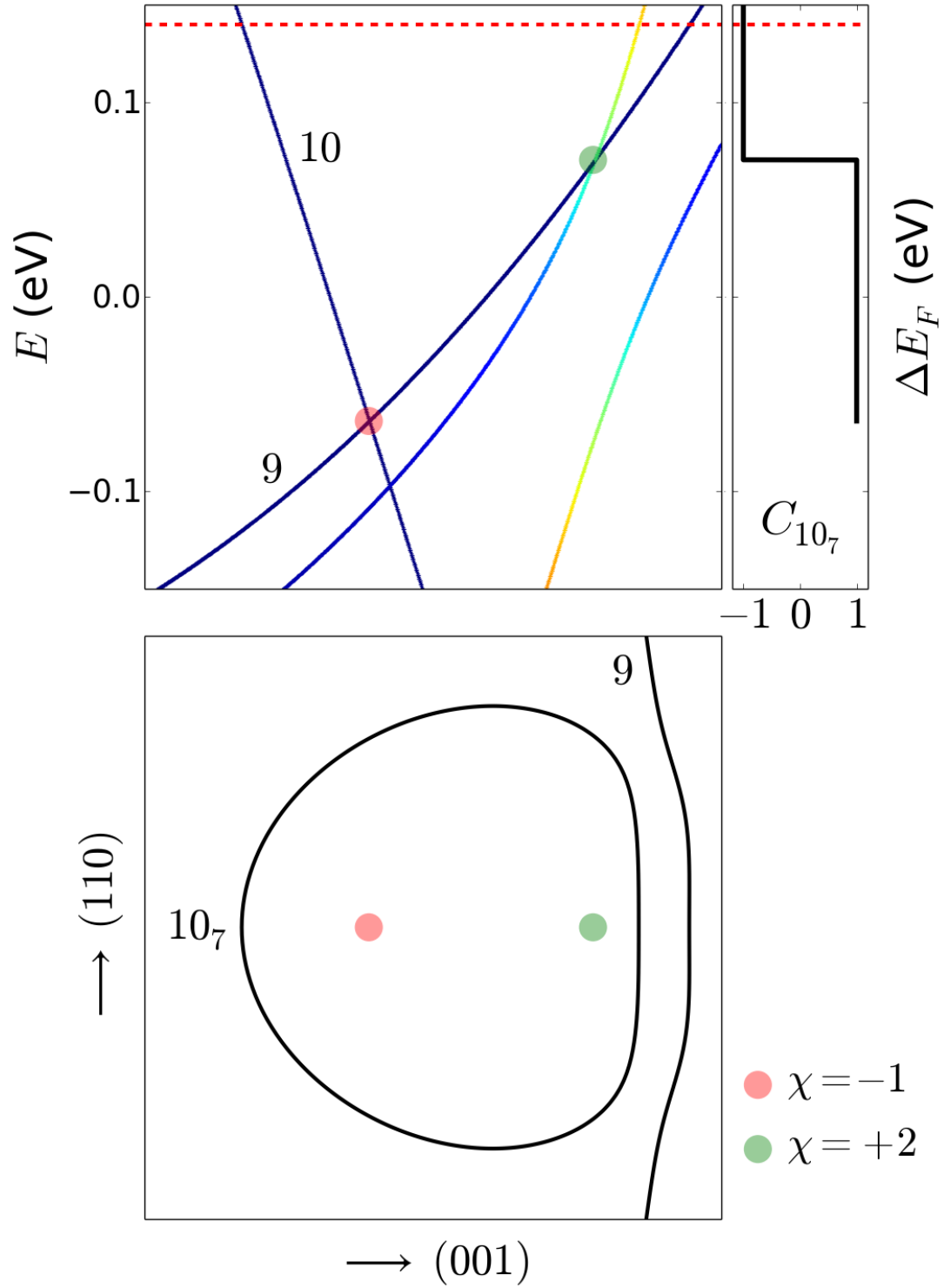


FIG. S25. Upper-left panel: Energy bands along the line  $\Delta$  in Fig. 3, close to the electron pocket  $10_7$  [see also Fig. 13(a)]. Energies are measured from the true Fermi level. Upper-right panel: Chern number of pocket  $10_7$  versus the Fermi-level shift. Lower panel: Fermi contours inside the red square in Fig. S20 for  $\Delta E_F = 0.140$  eV (the dashed red line in the upper panels). The red and green disks represent Weyl nodes between bands nine and ten, and  $\chi$  is the chiral charge.